Fluid Phase Equilibria 562 (2022) 113565

Contents lists available at ScienceDirect

Fluid Phase Equilibria

journal homepage: www.journals.elsevier.com/fluid-phase-equilibria

New insights and updated correlations for density, viscosity, refractive index, and associated properties of aqueous 4-diethyl-amino-2-butanol solution

Teerawat Sema [a,b,*], Hongxia Gao [c], Zhiwu Liang [c], Paitoon Tontiwachwuthikul [d], Raphael O. Idem [d]

[a] Department of Chemical Technology, Faculty of Science, Chulalongkorn University, Pathumwan, Bangkok, 10330, Thailand
[b] Center of Excellence on Petrochemical and Materials Technology, Chulalongkorn University, Pathumwan, Bangkok, 10330, Thailand
[c] Joint International Center for CO_2 Capture and Storage (iCCS), Provincial Hunan Key Laboratory for Cost-effective Utilization of Fossil Fuel Aimed at Reducing CO_2 Emissions, College of Chemistry and Chemical Engineering, Hunan University, Changsha, 410082, PR China
[d] Clean Energy Technologies Research Institute (CETRi), Faculty of Engineering and Applied Science, University of Regina, SK, S4S0A2, Canada

ARTICLE INFO

Keywords:
Density
Viscosity
Refractive index
Amine
Carbon capture

ABSTRACT

In this study, volumetric, viscometric, and refraction properties of binary 4-diethylamino-2-butanol (DEAB) and water mixture were comprehensively investigated over an entire range of amine concentration and a temperature range of 298.15-343.15 K. In addition to typical density, viscosity, refractive index, and their excess properties, the associated properties (including partial molar volume, apparent partial molar volume, partial molar volume and apparent partial molar volume at infinite dilution, thermal expansion coefficient, excess thermal expansion coefficient, Gibbs free energy, enthalpy, entropy, excess Gibbs free energy, and excess entropy for activation of viscous flow, molar polarizability, and molar free volume) were comprehensively considered. The obtained excess properties revealed that there was a strong contraction of liquid mixture through intermolecular interaction and/or preference molecular packing. Also, Gibbs free energy for activation of viscous flow was a key parameter affecting liquid viscosity. It was suggested that refractive index should be considered with density for a molar polarizability and a free molar volume for CO_2 physical solubility. Additionally, the Redlich-Kister equation was very effective for correlating the studied excess physical properties.

1. Introduction

An increase of the earth surface temperature has gone beyond the point of no return due to the anthropogenic carbon emission [1]. To mitigate this issue, the world leaders, by the scientific advisory, have pledged to limit an increase of the earth surface temperature at 1.5°C respecting the preindustrial period and become a carbon neutrality by or around 2050 [2, 3]. An amine-based technology is considered as one of the keys for achieving this global ambitious goal through carbon capture, utilization, and storage (CCUS) [4]. The technology has been commercially proved to be very promising for a large scale industrial decarbonization. Lessons learned from the world renowned BD3 SaskPower CCUS have revealed that the solvent management is vital for a succession of the project [5, 6].

One of the recent challenges for solvent management is to use a high efficiency amine [7, 8]. It has been reported that 4-diethylamino-2-butanol (DEAB) possesses a great potential as an alternative promising amine [9]. This is due to the fact that chemical structure of DEAB is strategically designed by appropriate substitution of the hydroxyl and alkyl groups in the amino alcohol structure. Maneeintr and co-workers [10] synthesized DEAB and experimentally measured fundamental physical properties (i.e., density, viscosity, and refractive index) of DEAB and water binary mixture over an entire range of amine concentration and a temperature range of 298.15-343.15 K. The reported data are useful for basic hydrodynamics design of the solvent in an absorption column and a gas-liquid contactor [11,12]. However, an insight discussion on the excess and associated properties has not yet been raised. Regarding the reported information, several additional volumetric, viscometric, and refraction properties (i.e., partial molar volume, partial molar volume at infinite dilution, apparent partial molar volume, apparent molar volume at infinite dilution, thermal expansion coefficient, excess thermal

* Corresponding author at: Department of Chemical Technology, Faculty of Science, Chulalongkorn University, Thailand
E-mail address: teerawat.se@chula.ac.th (T. Sema).

https://doi.org/10.1016/j.fluid.2022.113565
Received 10 May 2022; Received in revised form 25 July 2022; Accepted 1 August 2022
Available online 1 August 2022

Nomenclature

a_1	constant parameter for A_k (cm^3/mol)
a_2	constant parameter for A_k (cm^3/(mol.K))
a_3	constant parameter for A_k (cm^3/(mol.K^2))
b_1	constant parameter for B_k (1/K)
b_2	constant parameter for B_k (1/(K^2))
b_3	constant parameter for B_k (1/(K^3))
c_1	constant parameter for C_k (mPa.s)
c_2	constant parameter for C_k ((mPa.s)/K)
c_3	constant parameter for C_k ((mPa.s)/K^2)
c_4	constant parameter for C_k ((mPa.s)/K^3)
d_1	constant parameter for D_k (kJ/mol)
d_2	constant parameter for D_k (kJ/(mol.K))
d_3	constant parameter for D_k (kJ/(mol.K^2))
A_k	temperature dependent coefficient (cm^3/mol)
B_k	temperature dependent coefficient (1/K)
C_k	temperature dependent coefficient (mPa.s)
D_k	temperature dependent coefficient (kJ/mol)
f_m	molar free volume (cm^3/mol)
ΔG^*	Gibbs free energy for activation of viscous flow (kJ/mol)
ΔG^{*E}	excess Gibbs free energy for activation of viscous flow (kJ/mol)
h	Planck's constant (1.0546×10^{-34} J.s)
ΔH^*	enthalpy for activation of viscous flow (kJ/mol)
n_D	refractive index
n_D^E	excess refractive index
n_{Di}^0	refractive index of pure i
N	number of correlated data
N_A	Avogadro's number (6.0221×10^{23} 1/mol)
M	number of adjusting parameters
M_i	molecular weight of component i (g/mol)
R	universal gas constant (8.314 J/(mol.K))
R_m	molar polarizability (cm^3/mol)
ΔS^*	entropy for activation of viscous flow (J/(mol.K))
ΔS^{*E}	excess entropy for activation of viscous flow (J/(mol.K))
t	time (s)
T	temperature (K)
V_m^E	excess molar volume of mixture (cm^3/mol)
V_m	molar volume of mixture (cm^3/mol)
$V_{\varphi,i}$	apparent partial molar volume of component i (cm^3/mol)
V_i^0	molar volume of pure i (cm^3/mol)
$V_{\varphi,i}^{\infty}$	apparent molar volume at infinite dilution for component i (cm^3/mol)
$\overline{V}_i$	partial molar volume of component i (cm^3/mol)
$\overline{V}_i^{\infty}$	partial molar volume at infinite dilution (cm^3/mol)
x_i	mole fraction of component i (mol/mol)

Greek letters

α_m	volumetric thermal expansion coefficient (1/K)
α_i^0	volumetric thermal expansion coefficient of pure i (1/K)
α_m^E	excess volumetric thermal expansion coefficient (1/K)
η_m	viscosity of mixture (mPa.s)
η_i^0	viscosity of pure i (mPa.s)
η_m^E	excess viscosity (mPa.s)
ρ_m	density of mixture (g/cm^3)
ρ_i^0	density of pure i (g/cm^3)
σ	standard deviation of the prediction

expansion coefficient, activation energy for viscous flow, Gibbs free energy, enthalpy, entropy, excess Gibbs free energy, and excess entropy for activation of viscous flow, molar polarizability, and molar free volume) can be extracted.

The above-mentioned properties are essential for an insight understanding of the liquid equilibria. Additionally, they are very useful for a computational fluid dynamics simulation of the liquid flow inside the absorption column. To fulfill this knowledge gap, this work then determined these new data from the experimental densities, viscosities, and refractive indices reported by Maneeintr and colleagues [10]. Even though the predictive correlations for density, viscosity, and refractive index of binary DEAB and water mixture were proposed, they are applicable at specific temperatures of 298.15, 303.15, 313.15, 323.15, 333.15, and 343.15 K. An interpolation is needed at desired temperature within this temperature range. The updated Redlich-Kister based correlations were developed in this work to cover the calculation of the three basic physical properties and their excess values over an entire range of amine concentration and a temperature range of 298.15-343.15 K. Additionally, the correlations for estimating thermal expansion coefficient, excess thermal expansion coefficient, and excess Gibbs free energy of activation for viscous flow were also developed. The new insights and updated correlations, presented in this work, will be a strong fundamental for a better understanding of the fluid equilibria of an aqueous solution of DEAB.

2. Methods

2.1. Data collection and measurement uncertainty

The experimental data for density, viscosity, and refractive index of aqueous DEAB solution over a whole range of amine concentration and a temperature range of 298.15-343.15 K were collected from the work of Maneeintr et al. [10]. The detailed experimental description was reported in the literature [10]. DEAB was synthesized according to the procedure reported by Tontiwachwuthikul et al. [9]. Briefly, 65 ml of methyl vinyl ketone was added dropwise to 70 ml diethylamine in a well-stirred reactor at temperature below 273.15 K for 1 hour. The agitation was continued at room temperature for another 3 hours. Methanol (30 ml) was then added into the reactor. The system was again cooled down to 273.15 K, at which 26 g of sodium boron hydride was slowly added for 1 hour. The stirring was continued at room temperature for another 3 hours. Then, 30 ml of saturated sodium chloride solution was added into the reactor, which was continuously stirred for another 1 hour. The organic layer was separated then dried using sodium sulfate. After filtration, the organic liquid was fractionally distilled for DEAB. The 95% purity of DEAB was obtained based on the GC-MS analysis.

The experiment was conducted at atmospheric pressure. An aqueous DEAB solution was prepared by mixing the synthesized DEAB and the distilled water using analytical balance. The sources of uncertainty (which was considered in this work) are weight measurement, mole fraction measurement, temperature measurement, and repeatability. These four standard uncertainties were used to calculate the combined standard uncertainties (i.e., $u_c(\rho_m)$, $u_c(\eta_m)$, and $u_c(n_D)$) and the combined expanded uncertainties (i.e., $U_c(\rho_m)$, $U(\eta_m)$, and $U_c(n_D)$) according to the EURACHEM Quantify Uncertainty in Analytical Measurement [13]. Standard uncertainties of weight measurement ($u(w)$) and mole fraction measurement ($u(x)$) are 8×10^{-5} g and 0.0002, respectively. The liquid density at desired DEAB concentration was measured by Anton Parr DMA-4500 density meter over a temperature range of 298.15-343.15 K (standard uncertainties of temperature measurement ($u(T)$) and repeatability ($u(rep)$) are 0.006 K and 0.00002 g/cm^3, respectively). From the experimental reported densities, the combined

standard uncertainty for density $u_c(\rho_m)$ is 0.0025 g/cm^3. As a result, the combined expanded uncertainty for density measurement $U_c(\rho_m)$ is 0.005 g/cm^3 with 0.95 level of confidence (k ≈ 2). A glass Cannon-Ubbelohde viscometer (Cole-Parmer) was used for measuring the liquid kinematic viscosity. A standard uncertainty ($u(T)$) of 0.006 K was obtained from the temperature-controlled water bath (CT 500, Cannon Instrument). From the experiment, $u(rep)$ for viscosity measurement is 0.03 mPa.s. As a result, the combined standard uncertainty $u_c(\eta_m)$ and the combined expanded uncertainty $U_c(\eta_m)$ for dynamic viscosity measurement are 0.01 mPa.s and 0.02 mPa.s (at 0.95 level of confidence, k ≈ 2), respectively. The refractive index of aqueous DEAB solution was measured by an RX-5000-α refractometer (Atago Inc.) with $u(T)$ of 0.01 K and $u(rep)$ of 0.00005. The combined standard uncertainty $u_c(n_D)$ is 0.00005. Then, the combined expanded uncertainty for refractive index $U_c(n_D)$ was obtained at 0.0001 (0.95 level of confidence, k ≈ 2).

2.2. Prediction assessment

In this study, the density, excess molar volume, thermal expansion coefficient, excess thermal expansion coefficient, viscosity, excess viscosity, excess Gibbs free energy of activation for viscous flow, refractive index, and excess refractive index were estimated. To assess the prediction performance of the developed correlation, two performance indicators were used. They are an average absolute deviation percentage (%AAD) and a standard deviation of the prediction (σ). Ideally, %AAD and σ should approach zero. It should be noted that a relatively high σ may be obtained if too many fitting parameters are used. The two assessed indicators can be calculated from Eqs. (1) and (2), respectively.

$$\%AAD = \frac{1}{N}\sum_{j=1}^{N}\left|\frac{EXP_j - PRED_j}{EXP_j}\right| \times 100\% \quad (1)$$

$$\sigma = \left[\sum_{j=1}^{N}\frac{\left(EXP_j - PRED_j\right)^2}{N-M}\right]^{1/2} \quad (2)$$

where EXP_j is experimental measured value, $PRED_j$ is predicted value, N is number of correlated data, and M is number of adjusting parameters

3. Results and discussion

3.1. Volumetric properties

3.1.1. Density and molar volume

The collected experimental density of DEAB (1) and water (2) binary mixture at DEAB mole fraction (x_1) of 0.0000 to 1.0000 over a temperature range of 298.15-343.15 K are tabulated in Table 1 and plotted in Fig. 1. It was observed that the density of pure DEAB and aqueous DEAB solution decreased as the temperature increased. The reason is quite logical in that the thermal energy induces a liquid volume expansion [14]. As a result, the density, which is a ratio of mass per volume, then decreases accordingly. Additionally, the density of pure DEAB (ρ_1^0) can be correlated as a function of temperature in Kelvin (T) [15], as shown in Eq. (3), with %AAD and $\sigma(\rho_1^0)$ of 0.006% and 0.00007 g/cm^3, respectively. The results from Table 1 and Fig. 1 showed that the density of aqueous DEAB solution (ρ_m) decreased as the mole fraction of DEAB increased. This is because of ρ_1^0 is lower than ρ_2^0. It should also be pointed out that an aqueous solution of DEAB was found to be in two phases at relatively high water-content and temperature [9]. Table 1 and Fig. 1 illustrate that phase separation can be observed at (i) $x_1 \leq 0.1000$ at 323.15 K, (ii) $x_1 \leq 0.1999$ at 333.15 K, and (iii) $x_1 \leq 0.2989$ at 343.15 K.

$$\rho_1^0 = 1.1003 - \left(8.0716 \times 10^{-4}\right)T \quad (3)$$

Regarding the experimentally measured density, the molar volume

Table 1
ρ_m and V_m^E of binary mixture of DEAB (1) and water (2) at various temperatures.

x_1	ρ_m [(a)] (g/cm^3) 298.15 K	V_m^E (cm^3/mol)	ρ_m [(a)] (g/cm^3) 303.15 K	V_m^E (cm^3/mol)	ρ_m [(a)] (g/cm^3) 313.15 K	V_m^E (cm^3/mol)
0.0000	0.99705	0.000	0.99564	0.000	0.99220	0.000
0.1000	0.96241	-1.214	0.95822	-1.176	0.94944	-1.096
0.1999	0.93510	-1.759	0.93057	-1.712	0.92129	-1.612
0.2989	0.91715	-2.051	0.91259	-2.001	0.90334	-1.895
0.4000	0.90322	-2.121	0.89869	-2.069	0.88950	-1.954
0.5000	0.89367	-2.156	0.88916	-2.102	0.88101	-2.084
0.5991	0.88448	-1.903	0.88006	-1.854	0.87190	-1.835
0.6999	0.87521	-1.330	0.87091	-1.289	0.86219	-1.185
0.7955	0.86864	-0.827	0.86443	-0.795	0.85597	-0.717
0.8983	0.86271	-0.234	0.85860	-0.215	0.85038	-0.169
1.0000	0.85975	0.000	0.85573	0.000	0.84774	0.000
x_1	ρ_m [(a)] (g/cm^3) 323.15 K	V_m^E (cm^3/mol)	ρ_m [(a)] (g/cm^3) 333.15 K	V_m^E (cm^3/mol)	ρ_m [(a)] (g/cm^3) 343.15 K	V_m^E (cm^3/mol)
0.0000	0.98801	0.000	0.98318	0.000	0.97774	0.000
0.1000	N/A	N/A	N/A	N/A	N/A	N/A
0.1999	0.91164	-1.502	N/A	N/A	N/A	N/A
0.2989	0.89389	-1.784	0.88439	-1.678	N/A	N/A
0.4000	0.88024	-1.843	0.87081	-1.724	0.86133	-1.608
0.5000	0.87180	-1.965	0.86248	-1.842	0.85310	-1.719
0.5991	0.86276	-1.705	0.85355	-1.574	0.84419	-1.430
0.6999	0.85346	-1.087	0.84465	-0.988	0.83575	-0.882
0.7955	0.84748	-0.644	0.83892	-0.571	0.83028	-0.492
0.8983	0.84212	-0.126	0.83382	-0.089	0.82543	-0.043
1.0000	0.83969	0.000	0.83157	0.000	0.82340	0.000

N/A: not applicable due to phase separation of the solvent
Standard uncertainties: $u(x) = 0.0002$, $u(T) = 0.006\ K$, $u(w) = 0.00008\ g$, and $u(rep) = 0.00002\ g/cm^3$
Combined expanded uncertainties: $U_c(\rho_m) = 0.005 g/cm^3$ and $U_c(V_m^E) = 0.05 cm^3/mol$ with 0.95 level of confidence (k ≈ 2)
[(a)] Data obtained from Maneeintr et al. [10]

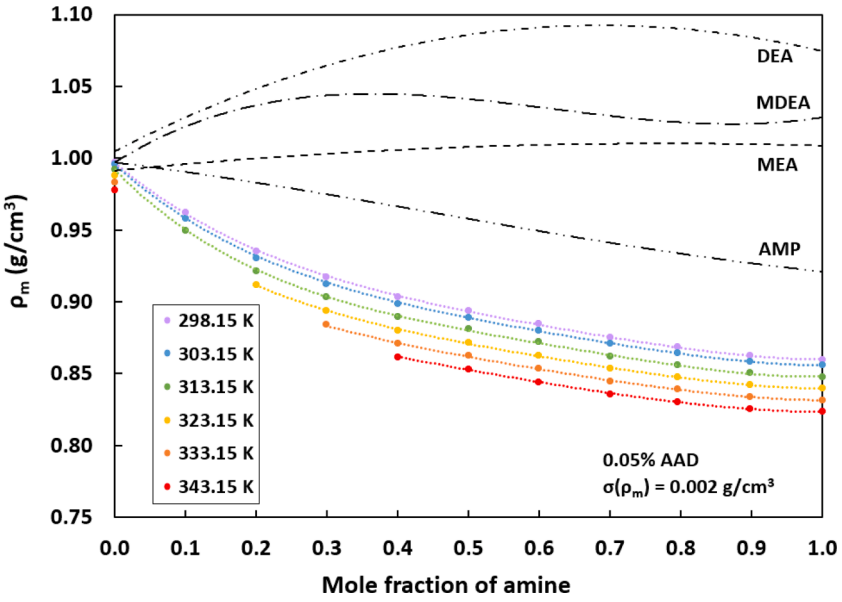

Fig. 1. ρ_m of aqueous solutions of DEAB over ranges of concentration and temperature; dots are experimental data, color dashed lines are predicted results, and black dashed lines are density of conventional amines at 313.15 K [18–21].

(V_m) can be determined, as given in Eq. (4). The calculated V_m of DEAB and water binary mixture over a whole range of concentration and a temperature range of 298.15-343.15 K are presented in Table S1 (in the Supplementary Material). Since ρ_m decreased as the temperature increased, V_m then slightly increased as the temperature increased at a specific DEAB concentration. It was also noticed that an increase of DEAB mole fraction resulted in a considerable increase of V_m. This is due to the fact that the molecular weight of DEAB (145.240 g/mol) is much higher than that of water (18.015 g/mol). In addition to V_m, the excess molar volume (V_m^E) can be calculated as a deviation of V_m for the real mixture and that for the ideal mixture as shown in Eq. (5).

$$V_m = \frac{\sum_{i=1}^{n}(x_i M_i)}{\rho_m} \tag{4}$$

$$V_m^E = V_m - \sum_{i=1}^{n}\left(x_i V_i^0\right) \tag{5}$$

where V_i^0 is molar volume of pure component i, M_i is molecular weight of component i, and n is number of components

The calculated V_m^E of an aqueous DEAB solution at various concentrations and temperatures are presented in Table 1 and plotted in Fig. 2. The results showed that V_m^E were in a negative range and varied with the DEAB concentration and temperature. The negative V_m^E refers that V_m of the real mixture is less than that of the ideal mixture according to Eq. (5). In other words, there should be a contraction of the real liquid mixture. This contraction is a consequence of the intermolecular interaction (e.g., dipole interaction and H-bonding) and the compact molecular packing

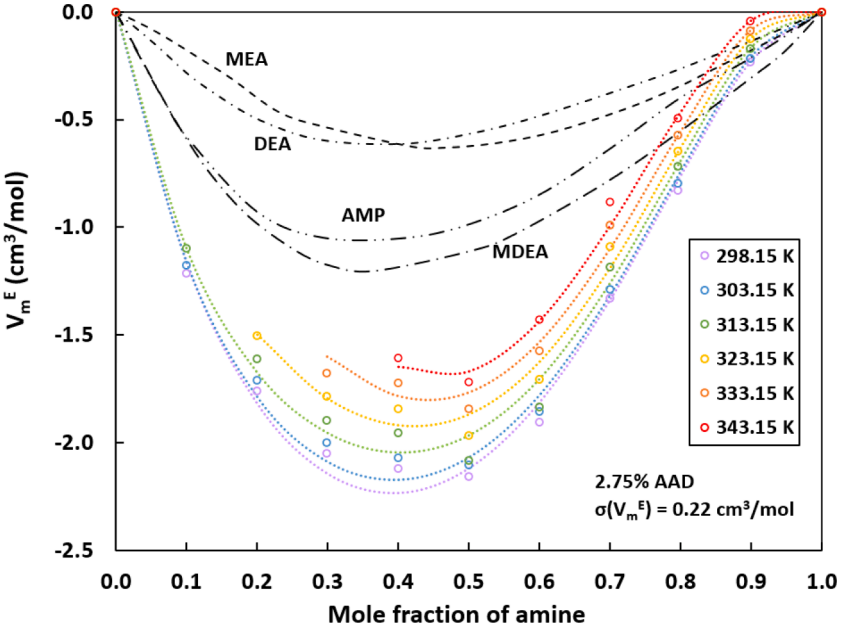

Fig. 2. V_m^E of aqueous solutions of DEAB over ranges of concentration and temperature; open dots are V_m^E obtained from Eq. (5), color dashed lines are predicted results from the Redlich-Kister equation, and black dashed lines are V_m^E of conventional amines at 313.15 K [19–21].

of the liquid mixture [16]. For the effect of temperature, Table 1 and Fig. 2 reveal that V_m^E decreases as the temperature increases. Bearing in mind that at an elevated temperature, (i) the intermolecular interaction is weakened and (ii) the liquid molecule gains more kinetic energy. Thus, the molecular contraction of liquid mixture is then loosened. For the effect of DEAB concentration, it was observed that V_m^E decreased to its minimum ($x_1 \sim 0.5$) then increased as x_1 increased. In other words, the liquid contraction increased to its maximum ($x_1 \sim 0.5$) then decreased as x_1 increased. It can be implied from this observation that there should be the strongest intermolecular interaction and/or the most suitable molecular packing at a certain component mixture (in this case, $x_1 \sim 0.5$). Interestingly, the maximum concentration was not largely affected by the temperature as illustrated in Fig. 2. In comparison with the conventional amines (i.e., monoethanolamine (MEA), diethanolamine (DEA), *N*-methyldiethanolamine (MDEA), and 2-amino-2methyl-1-propanol (AMP)) at 313.15 K, it was found that the aqueous solution of DEAB possessed more negative value of V^E than that of MDEA, AMP, DEA, and MEA, respectively. This suggested that the molecular contraction of the aqueous DEAB solution was stronger than that of MDEA, AMP, DEA, and MEA, respectively.

In this work, the Redlich-Kister equation was applied for a prediction of V_m^E for DEAB aqueous solution over the studied ranges of concentration and temperature. The Redlich-Kister based correlation for V_m^E is presented in Eq. (6) as a function of x_1 and temperature dependent coefficient (A_k) [17]. It should be noted that A_k is a polynomial function with temperature T, as given in Eq. (7).

$$V_m^E = (2x_1 - 1)\sum_{k=1}^{m}\left[A_k(2x_1 - 1)^{k-1}\right] \tag{6}$$

$$A_k = \sum_{k'=1}^{m'}\left[a_{k'}T^{k'-1}\right] \tag{7}$$

Based on the V_m^E results presented in Table 1, a non-linear regression was used to fit the adjusting constant parameters ($a_{k'}$). In this case, m was set at four ($m = 4$) for Eq. (6), while second-order polynomial function ($m' = 3$) was applied for Eq. (7). As a result, the fitted constant parameters ($a_{k'}$) of temperature dependent coefficient A_k for a prediction of V_m^E are presented in Table 2. The predicted V_m^E based on Eqs. (6) and (7) are presented in Fig. 2 as color deashed lines. It can be clearly seen that the predicted results are in very good agreement with the values of V_m^E (obtained from Eq. (5)) with %AAD of 2.75% and $\sigma(V_m^E)$ of 0.22 cm^3/mol.

Regarding a prediction of V_m^E from the Redlich-Kister based correlation, the predicted V_m^E can be used to estimate ρ_m through Eqs. (4) and (5). The predicted ρ_m are plotted as color dashed lines against the experimental data (dots), as shown in Fig. 1. It was found that the predicted ρ_m very well corresponded with the experimental ρ_m with %AAD of 0.05% and $\sigma(\rho_m)$ of 0.002 g/cm^3. It is worth mentioning that at a higher degree of the Redlich-Kister equation (in other words, m in Eq. (6) is increased from 4 to 5), %AAD for V_m^E is found to decrease from 2.75% to 2.63%, but that for ρ_m does not change (0.05%). However, an increase of the number of the adjusting parameters negatively affects σ in that $\sigma(V_m^E)$ increases from 0.22 cm^3/mol to 0.28 g/cm^3 and $\sigma(\rho_m)$ increases from 0.002 g/cm^3 to 0.003 g/cm^3. On the other hand, if three adjusting parameters ($m = 3$) are considered, the prediction performance becomes poorer than the case of four adjusting parameters ($m = 4$). In the case of $m = 3$, %AADs for V_m^E and ρ_m are 4.73% and 0.10%, while $\sigma(V_m^E)$ and $\sigma(\rho_m)$ are 0.58 cm^3/mol and 0.006 g/cm^3, respectively. Hence, the four adjusting parameters ($m = 4$) for the Redlich-Kister equation (Eq. (6)) was then selected in this work.

Table 2
Constant parameters for the temperature dependent coefficient (A_k).

Temperature dependent coefficient (A_k)	Constant parameter	
A_1	a_1	-2.1151×10^{1}
	a_2	4.4790×10^{-2}
	a_3	-7.5205×10^{-6}
A_2	a_1	6.2206×10^{1}
	a_2	-3.2381×10^{-1}
	a_3	4.3401×10^{-4}
A_3	a_1	3.2454×10^{2}
	a_2	-2.1284
	a_3	3.5008×10^{-3}
A_4	a_1	-5.0040×10^{2}
	a_2	3.2132
	a_3	-5.1078×10^{-3}

According to the presented data of ρ_m, V_m and V_m^E, several additional fundamental volumetric properties can also be determined [21–23]. Partial molar volume of component i, which is either DEAB (1) or water (2), can be calculated from Eqs. (8) and (9) through the Redlich-Kister temperature dependent coefficient A_k for a prediction of V_m^E [24]. It should be noted that according to Eq. (6), m is set at four ($m = 4$).

$$\overline{V}_1 = V_1^0 + (1 - x_1)\sum_{k=1}^{m}A_k(2x_1 - 1)^{k-1} - 2x_1(1 - x_1)\sum_{k=1}^{m}A_k(k-1)(2x_1 - 1)^{k-2} \tag{8}$$

$$\overline{V}_2 = V_2^0 + (1 - x_2)^2\sum_{k=1}^{m}A_k(1 - 2x_2)^{k-1} + 2x_2(1 - x_2)^2\sum_{k=1}^{m}A_k(k-1)(1 - 2x_2)^{k-2} \tag{9}$$

The calculated partial molar volume of DEAB ($\overline{V}_1$) and that of water ($\overline{V}_2$) over an entire range of DEAB concentration and a temperature range of 298.15-343.15 K are given in Table S1 (in the Supplementary Material). Regarding these data, the partial molar volume at infinite dilution of DEAB ($\overline{V}_1^{\infty}$) and that of water ($\overline{V}_2^{\infty}$) can be determined by letting $x_1 = 0$ in Eq. (8) and $x_2 = 0$ in Eq. (9), respectively. As a result, the much simpler equations for calculating $\overline{V}_1^{\infty}$ and $\overline{V}_2^{\infty}$ can be written as Eqs. (10) and (11), respectively. The predicted values of $\overline{V}_1^{\infty}$ and $\overline{V}_2^{\infty}$ over a range of studied temperature are tabulated in Table 3.

$$\overline{V}_1^{\infty} = V_1^0 + \sum_{k=1}^{m}A_k(-1)^{k-1} \tag{10}$$

$$\overline{V}_2^{\infty} = V_2^0 + \sum_{k=1}^{m}A_k \tag{11}$$

$$V_{\varphi,i} = V_i^0 + \left(\frac{V^E}{x_i}\right) \tag{12}$$

As can be seen that the above-mentioned procedure for a calculation of $\overline{V}_i$ and $\overline{V}_i^{\infty}$ strongly depends on the temperature dependent coefficient A_k. So that the Redlich-Kister based predictive correlation for V_m^E needs to be initially established. To simplify this calculation procedure, an alternative approach through the apparent partial molar volume ($V_{\varphi,i}$) can be applied [22]. In this case, the apparent partial molar volumes of DEAB ($V_{\varphi,1}$) and water ($V_{\varphi,2}$) can be determined through Eq. (12) using their V_i^0, V_m^E, and x_i. Regarding Eq. (12), $V_{\varphi,i}^{\infty}$ cannot be calculated by letting $x_i = 0$. Hence, an extrapolation of $V_{\varphi,i}$ to the infinite dilution (x_i approaches zero) must be conducted. The calculated $V_{\varphi,1}$ and $V_{\varphi,2}$ at various concentrations and temperatures are given in Table S1 (in the Supplementary Material). Additionally, the extrapolated results to an infinite dilution for DEAB ($V_{\varphi,1}^{\infty}$) and water ($V_{\varphi,2}^{\infty}$) are presented in Table 3. It was found that (i) the values of $V_{\varphi,i}$ were in good agreement with that of $\overline{V}_i$, as presented in Table S1 (in the Supplementary Material), and (ii) the values of $V_{\varphi,i}^{\infty}$ were close to that of $\overline{V}_i^{\infty}$ for both infinite

Table 3
V_i^0, $\overline{V}_i^\infty$, and $V_{\varphi,i}^\infty$ for binary system of DEAB (1) and water (2) over 298.15-343.15 K.

Temperature (K)	$V_1^0(cm^3/mol)$	$\overline{V}_1^\infty(cm^3/mol)$	$V_{\varphi,1}^\infty(cm^3/mol)$	$V_2^0(cm^3/mol)$	$\overline{V}_2^\infty(cm^3/mol)$	$V_{\varphi,2}^\infty(cm^3/mol)$
298.15	168.654	153.551	154.668	18.068	18.552	16.258
303.15	169.446	154.021	155.874	18.094	19.059	16.475
313.15	171.043	156.197	158.429	18.157	19.907	17.088
323.15	172.683	160.049	161.989	18.234	20.534	18.283
333.15	174.369	165.581	164.334	18.323	20.937	18.157
343.15	176.099	172.791	165.956	18.425	21.117	18.937

dilutions of DEAB ($x_1 = 0$) and water ($x_2 = 0$), as shown in Table 3. In other words, $V_{\varphi,i}$ and $V_{\varphi,i}^\infty$ are well representing $\overline{V}_i$ and $\overline{V}_i^\infty$, respectively.

3.1.2. Thermal expansion coefficient

To obtain a better understanding of an isotropic change of the liquid volume by changing a temperature at isobaric condition, the volumetric thermal expansion coefficient (α_m) was considered. Based on its definition, α_m can be calculated by Eq. (13) [25]. Since V_m is associated with V_m^E and ideal mixture molar volume or $\sum_{i=1}^{n}(x_i V_i^0)$ (as shown in Eq. (5)), the differentiation of V_m with respecting T leads to Eq. (14). It should be indicated that Eq. (13) is preferable for the pure DEAB by considering V_m to be V_1^0, while Eq. (14) is favorable for the aqueous DEAB solution.

$$\alpha_m = \frac{1}{V_m}\left(\frac{\partial V_m}{\partial T}\right)_{P,x_i} \tag{13}$$

$$\alpha_m = \frac{1}{V_m}\left(\left(\frac{\partial V^E}{\partial T}\right)_{P,x_i} + \sum_{i=1}^{2}\left(\alpha_i^0 x_i V_i^0\right)\right) \tag{14}$$

In the case of pure DEAB and water, V_1^0 and V_2^0 (obtained from Table 3) were used to determine α_1^0 and α_2^0 through Eq. (13). The results are tabulated in Table 4 and correlated as a function of T, as shown in Eqs. (15) and (16), respectively. It was found that the calculated α_1^0 values using Eq. (15) were in very good agreement with the data obtained from Eq. (13) with %AAD of 0.02% and $\sigma(10^3\cdot\alpha_1^0)$ of 2.6×10^{-4} $(1000/K)$. Also, the calculated α_2^0 using Eq. (16) well corresponded with (i) the results obtained from Eq. (13) with %AAD of 0.07 % and $\sigma(10^3\cdot\alpha_2^0)$ of 3.4×10^{-4} $(1000/K)$ and (ii) the literature data [26] with %AAD of 3.26 % and $\sigma(10^3\cdot\alpha_2^0)$ of 1.5×10^{-2} $(1000/K)$.

$$\alpha_1^0 = \left(6.6458 \times 10^{-4}\right) + \left(9.1946 \times 10^{-7}\right)T \tag{15}$$

$$\alpha_2^0 = \left(3.7260 \times 10^{-4}\right) + \left(1.8730 \times 10^{-7}\right)T \tag{16}$$

For the aqueous DEAB solution, α_m was calculated using Eq. (14) based on the Redlich-Kister equation for V_m^E of Eq. (6). Be noted that α_1^0 and α_2^0 was determined from Eqs. (15) and (16), respectively. As a result, α_m of binary DEAB and water mixture are presented in Table 4 and Fig. 3. It was found that the values of α_1^0 and α_m were positive and increased as the temperature increased. This observation indicated that the liquid volume expands as the temperature increases. An increment of the liquid volume associated with a weakening of the intermolecular interaction and a loosening of the molecular packing. Additionally, it can be seen from Table 4 and Fig. 3 that α_m of aqueous DEAB solution varies with the DEAB concentration in that α_m rapidly increases over x_1

Table 4
α_m and α_m^E of binary mixture of DEAB (1) and water (2) at various temperatures.

x_1	$10^3\cdot\alpha_m$ $(1000/K)$ 298.15 K	$10^3\cdot\alpha_m^E$ $(1000/K)$	$10^3\cdot\alpha_m$ $(1000/K)$ 303.15 K	$10^3\cdot\alpha_m^E$ $(1000/K)$	$10^3\cdot\alpha_m$ $(1000/K)$ 313.15 K	$10^3\cdot\alpha_m^E$ $(1000/K)$
0.0000	0.429	0.000	0.429	0.000	0.431	0.000
0.1000	0.656	-0.033	0.784	0.093	1.039	0.341
0.1999	0.911	0.125	0.986	0.196	1.132	0.335
0.2989	1.032	0.195	1.059	0.218	1.112	0.263
0.4000	1.051	0.183	1.056	0.184	1.067	0.186
0.5000	1.021	0.132	1.024	0.130	1.031	0.129
0.5991	0.982	0.077	0.989	0.081	1.005	0.088
0.6999	0.958	0.042	0.969	0.048	0.990	0.060
0.7955	0.957	0.032	0.966	0.036	0.984	0.045
0.8983	0.962	0.030	0.966	0.029	0.974	0.028
1.0000	0.939	0.000	0.943	0.000	0.952	0.000
x_1	$10^3\cdot\alpha_m$ $(1000/K)$ 323.15 K	$10^3\cdot\alpha_m^E$ $(1000/K)$	$10^3\cdot\alpha_m$ $(1000/K)$ 333.15 K	$10^3\cdot\alpha_m^E$ $(1000/K)$	$10^3\cdot\alpha_m$ $(1000/K)$ 343.15 K	$10^3\cdot\alpha_m^E$ $(1000/K)$
0.0000	0.433	0.000	0.435	0.000	0.437	0.000
0.1000	N/A	N/A	N/A	N/A	N/A	N/A
0.1999	1.275	0.471	N/A	N/A	N/A	N/A
0.2989	1.163	0.307	1.215	0.350	N/A	N/A
0.4000	1.077	0.189	1.088	0.191	1.099	0.193
0.5000	1.037	0.126	1.043	0.123	1.049	0.120
0.5991	1.020	0.093	1.035	0.099	1.049	0.105
0.6999	1.011	0.072	1.032	0.084	1.053	0.096
0.7955	1.001	0.054	1.019	0.063	1.037	0.071
0.8983	0.983	0.028	0.991	0.027	1.000	0.026
1.0000	0.961	0.000	0.971	0.000	0.980	0.000

N/A: not applicable due to phase separation of the solvent
Standard uncertainties: $u(x) = 0.0002$, $u(T) = 0.006\ K$, and $u(w) = 0.00008\ g$
Combined expanded uncertainties: $U_c(10^3\cdot\alpha_m) = 0.001\ (1000/K)$ and $U_c(10^3\cdot\alpha_m^E) = 0.001(1000/K)$ with 0.95 level of confidence ($k \approx 2$)

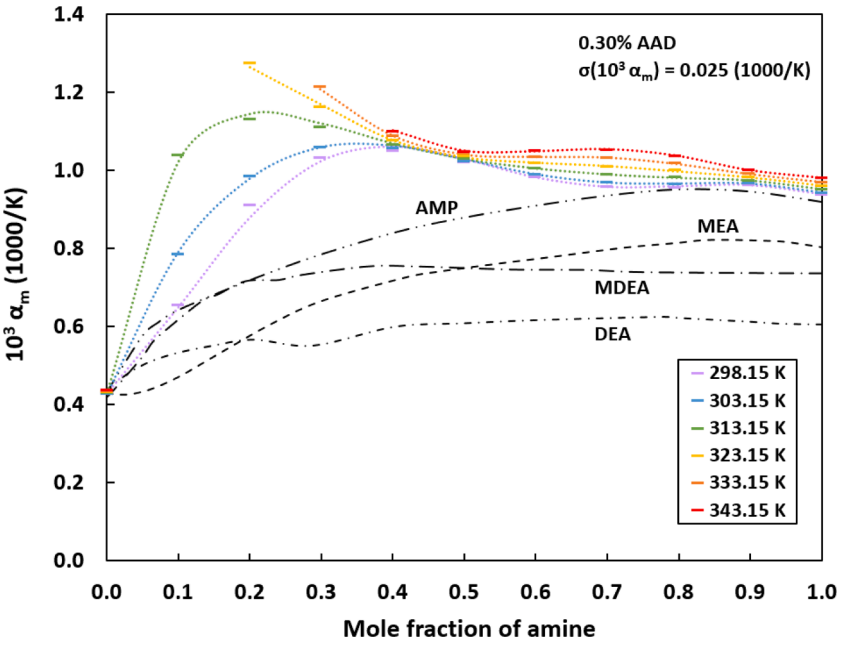

Fig. 3. α_m of aqueous solutions of DEAB over ranges of concentration and temperature; rectangulars are α_m obtained from Eq. (14), color dashed lines are predicted results, and black dashed lines are α_m of conventional amines at 313.15 K calculated from literature density data [20, 21, 26].

range of 0.0000 to 0.1999 within a temperature range of 298.15-313.15 K. Then, α_m slightly decreases as x_1 further increases.

There is a point of discussion regarding α_m and phase separation behavior in that the increment of liquid volume as an increase of temperature (which is α_m) is found to be relatively high at $x_1 < 0.2989$ and $T > 313.15$ *K*. Especially, at the phase separation region, a large increase of α_m may induce the liquid mixture to separate into two immiscible liquid phases. In comparison with the conventional amine solvents, the aqueous solution of DEAB possesses greater α_m than that of AMP, MEA, MDEA, and DEA, respectively. An increasing trend of α_m at a low amine concentration for aqueous DEAB solution is much sharper than that for conventional amines. Hence, the conventional amines can maintain as homogeneous liquid mixtures, but the aqueous DEAB solution separates into two liquid phases at relatively low DEAB concentration and relatively high temperature. The investigation of V_m^E also suggested that the molecular interaction is weakened, and the molecular compactness is loosened as the temperature increases. Bearing in mind that the DEAB molecule contains both hydrophilic amino and hydroxyl groups, and hydrophobic hydrocarbon groups. At a temperature range of 298.15-313.15 K, there is no phase separation because the intermolecular interaction and the molecular compactness are strong enough to homogenize the liquid mixture. However, as the temperature is increased to 323.15 K, the phase separation can be detected at $x_1 \leq 0.1000$. This is due to the weakening of the molecular interaction and the loosening of the molecular compactness regarding the increase of temperature. Hence, the liquid mixture separates into the aqueous phase and the organic phase. Interestingly, as the temperature is further increased to 333.15 K and 343.15 K, the phase separation occurs at a higher DEAB concentration of $x_1 \leq 0.1999$ and $x_1 \leq 0.2989$, respectively. It is because an increase of hydrophobicity in the liquid mixture. To gain more comprehensive view on the phase separation condition and mechanism, an in-dept investigation should be further investigated.

The Redlich-Kister equation was again applied for estimating α_m through an excess volumetric thermal expansion coefficient (α_m^E), which is defined as a deviation of the actual α_m and the ideal volumetric based mixing of liquid, as shown in Eq. (17). Regarding its definition, α_m^E data are tabulated in Table 4. As a result, α_m^E predictive correlation, which is a function of x_1 and temperature dependent coefficient (B_k), was developed as shown in Eq. (18). By applying a non-linear regression, the constant parameter $b_{k'}$ (see Eq. (19)) was obtained and given in Table 5. The predicted results (with $m = 5$ and $m' = 3$) are illustrated as color dashed lines in Fig. 4. The results showed that most of α_m^E values were positive (which means that α_m of the real mixture is greater than that of the ideal mixture). Only some negative α_m^E data were observed at 298.15 K, as illustrated in Fig. 4. Additionally, it was observed that α_m^E of the aqueous solution of DEAB was higher than that of MDEA, DEA, AMP, and MEA, respectively (especially, at a low range of x_1). Fig. 4 clearly shows that the predicted α_m^E data from the Redlich-Kister based correlation (Eq. (18)) are in good agreement with the data obtained from Eq. (17) with %AAD of 2.26% and $\sigma(10^3 \cdot \alpha_m^E)$ of 0.025 (1000/K).

$$\alpha_m^E = \alpha_m - \sum_{i=1}^{2}\left(\alpha_i^0 \frac{x_i V_i^0}{x_1 V_1^0 + x_2 V_2^0}\right) \tag{17}$$

$$\alpha_m^E = (2x_1 - 1)\sum_{k=1}^{m}\left[B_k (2x_1 - 1)^{k-1}\right] \tag{18}$$

Table 5
Constant parameters for temperature dependent coefficient (B_k).

Temperature dependent coefficient (B_k)	Constant parameter	
B_1	b_1	5.8724×10^{-3}
	b_2	-3.2008×10^{-5}
	b_3	4.7531×10^{-8}
B_2	b_1	-3.8187×10^{-2}
	b_2	2.2059×10^{-4}
	b_3	-3.2504×10^{-7}
B_3	b_1	-8.5943×10^{-2}
	b_2	4.7796×10^{-4}
	b_3	-6.3364×10^{-7}
B_4	b_1	4.9429×10^{-1}
	b_2	-2.9352×10^{-3}
	b_3	4.3149×10^{-6}
B_5	b_1	-4.2259×10^{-1}
	b_2	2.5719×10^{-3}
	b_3	-3.8924×10^{-6}

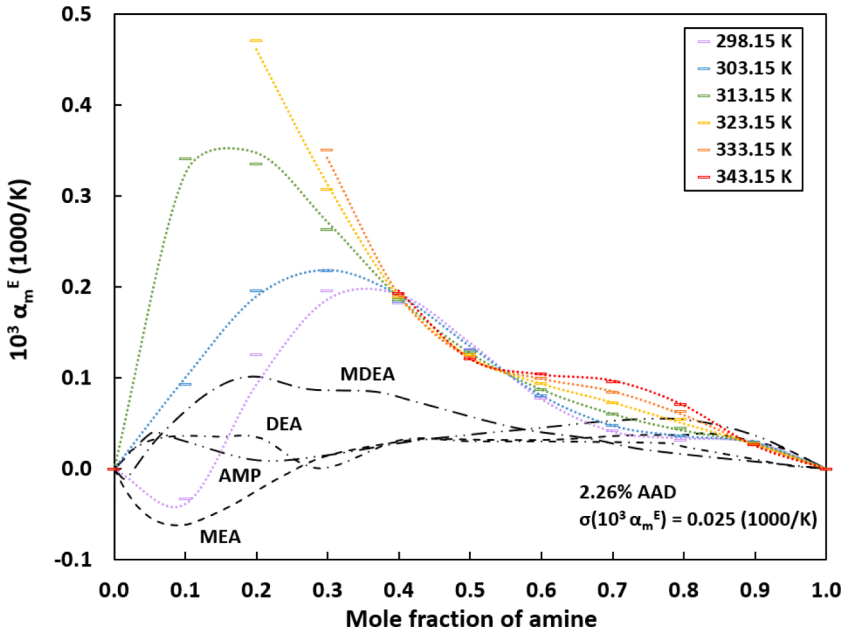

Fig. 4. α_m^E of aqueous solutions of DEAB over ranges of concentration and temperature; open rectangulars are α_m^E obtained from Eq. (17), color dashed lines are predicted results from the Redlich-Kister equation, and black dashed lines are α_m^E of conventional amines at 313.15 K calculated from literature density data [20, 21, 26].

$$B_k = \sum_{k'=1}^{m'} \left[b_{k'} T^{k'-1} \right] \tag{19}$$

3.2. Viscometric properties

3.2.1. Viscosity

The collected experimental viscosity data of the binary DEAB and water mixture over an entire range of concentration and a temperature range of 298.15-343.15 K are reported in Table 6 and Fig. 5. Regarding these data, the viscosity of pure DEAB (η_1^0) can be correlated as shown in Eq. (20). The results showed that the predicted η_1^0 values were well corresponding with the experimental data with %AAD of 1.58% and $\sigma(\eta_1^0)$ of 2.2 $\times 10^{-4}$ mPa.s.

$$\eta_1^0 = \left(8.3011 \times 10^{1}\right) - \left(4.7012 \times 10^{-1}\right)T + \left(6.7386 \times 10^{-4}\right)T^2 \tag{20}$$

The results from Table 6 and Fig. 5 also revealed that the viscosities of pure DEAB (η_1^0) and aqueous DEAB solution (η_m) decreased as the temperature increased. The reason is quite logical in that at an elevated temperature, there is a higher thermal energy for liquid to conquer the flow resistance. For the effect of DEAB concentration, it was found that an increase of x_1 resulted in an increase of η_m to the maximum level then decreased to η_1^0. Interestingly, this maximum η_m seemed to be independent of temperature and was found at $x_1 \sim 0.3$, as illustrated in Fig. 5. It can also be observed that the maximum η_m of aqueous DEAB solution at 313.15 K is lower than that of aqueous MEA solution and much lower than that of aqueous MDEA, AMP, and DEA solutions, respectively. However, at the typically used amine concentration of 30% wt. (which is equivalent to mole fraction of 0.05 for DEAB, 0.11 for MEA, 0.07 for DEA, 0.06 for MDEA, and 0.08 for AMP), η_m of the DEAB mixture is clearly higher than that of the conventional amine mixtures. So that the effect of η_m of DEAB mixture at various concentrations on the CO_2 absorption performance should be further investigated based on the data presented in this work.

Regarding the experimental η_m of aqueous DEAB solution (given in Table 6), the prediction of η_m can be conducted through η_m^E. With the same excess property concept as V_m^E and α_m^E, η_m^E can be expressed as Eq. (21) [30]. The calculated η_m^E of aqueous DEAB solution over the ranges of studied concentration and temperature are presented in Table 6 and Fig. 6. It was found that η_m^E varied with the temperature and amine concentration within a positive region. This means the viscous flow resistance of a real mixture is greater than that of an ideal mixture. The

Table 6
η_m and η_m^E of binary mixture of DEAB (1) and water (2) at various temperatures.

x_1	η_m [(a)] (mPa·s) 298.15 K	η_m^E (mPa·s)	η_m [(a)] (mPa·s) 303.15 K	η_m^E (mPa·s)	η_m [(a)] (mPa·s) 313.15 K	η_m^E (mPa·s)
0.0000	0.891	0.000	0.799	0.000	0.654	0.000
0.1000	7.961	6.884	6.310	5.345	4.158	3.387
0.1999	14.030	12.767	10.540	9.409	6.406	5.518
0.2989	16.610	15.162	12.350	11.055	6.730	5.726
0.4000	14.920	13.284	11.160	9.697	6.125	5.002
0.5000	10.960	9.138	8.334	6.705	5.159	3.919
0.5991	8.424	6.417	6.565	4.771	4.203	2.847
0.6999	6.280	4.086	5.020	3.059	3.397	1.923
0.7955	4.689	2.317	3.880	1.760	2.765	1.179
0.8983	3.552	0.988	3.037	0.747	2.265	0.558
1.0000	2.753	0.000	2.459	0.000	1.826	0.000
x_1	η_m [(a)] (mPa·s) 323.15 K	η_m^E (mPa·s)	η_m [(a)] (mPa·s) 333.15 K	η_m^E (mPa·s)	η_m [(a)] (mPa·s) 343.15 K	η_m^E (mPa·s)
0.0000	0.551	0.000	0.470	0.000	0.407	0.0000
0.1000	N/A	N/A	N/A	N/A	N/A	N/A
0.1999	4.261	3.524	N/A	N/A	N/A	N/A
0.2989	4.332	3.503	2.978	2.286	N/A	N/A
0.4000	3.968	3.045	2.755	1.988	2.005	1.3524
0.5000	3.412	2.396	2.411	1.570	1.793	1.0790
0.5991	2.898	1.789	2.105	1.190	1.538	0.7632
0.6999	2.434	1.231	1.758	0.768	1.365	0.5283
0.7955	2.062	0.770	1.538	0.477	1.230	0.3346
0.8983	1.696	0.309	1.353	0.216	1.103	0.1444
1.0000	1.482	0.000	1.213	0.000	1.021	0.0000

N/A: not applicable due to phase separation of the solvent
Standard uncertainties: $u(x) = 0.0002$, $u(T) = 0.006$ K, $u(w) = 0.00008$ g, and $u(rep) = 0.003$ g/cm^3
Combined expanded uncertainties: $U_c(\eta_m) = 0.02$ $mPa{\cdot}s$ and $U_c(\eta_m^E) = 0.03$ $mPa{\cdot}s$ with 0.95 level of confidence (k ≈ 2)
[(a)] Data obtained from Maneeintr et al. [10]

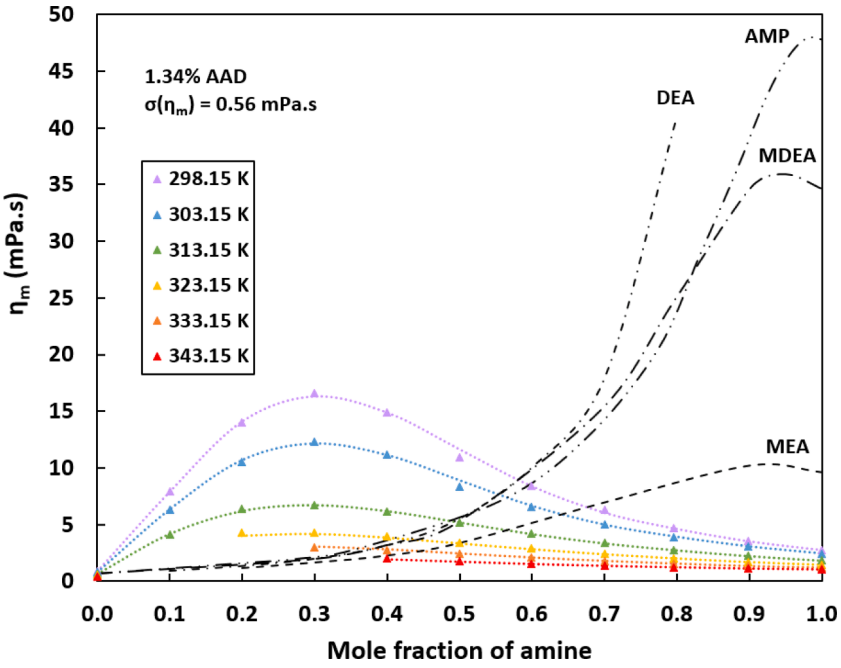

Fig. 5. η_m of aqueous solutions of DEAB over ranges of concentration and temperature; triangles are experimental data, color dashed lines are predicted results, and black dashed lines are viscosity of conventional amines at 313.15 K [21, 27-29].

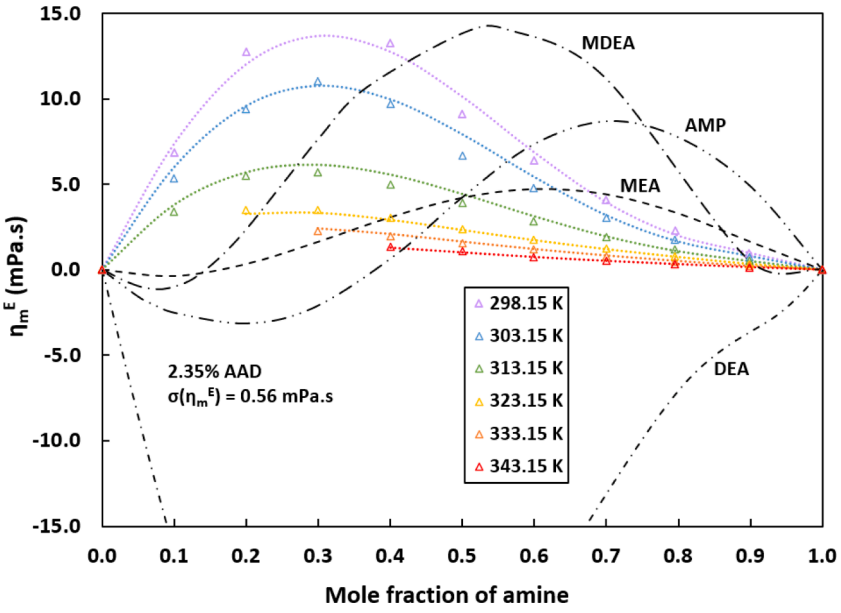

Fig. 6. η_m^E of aqueous solutions of DEAB over ranges of concentration and temperature; open triangles are η_m^E obtained from Eq. (21), color dashed lines are predicted results from the Redlich-Kister equation, and black dashed lines are η_m^E of conventional amines at 313.15 K [21, 31, 32].

literature also suggests that a positive η_m^E indicates a strong intermolecular force in the liquid mixture [24, 28]. Hence, there is a contraction of the binary mixture of DEAB and water. This statement is well corresponding to the negative values of V_m^E, presented in Table 1 and Fig. 2.

For the effect of temperature, it was found that η_m^E decreased as the temperature increased (see Table 6 and Fig. 6). Since η_m^E is defined as the viscosity deviation of a real mixture from an ideal mixture, a decrease of η_m^E means the viscous flow behavior of the real mixture is getting closer to that of the ideal mixture. This is because of a weakening of the intermolecular interaction (a major contribution) and a loosening of the molecular compactness (a minor contribution) at elevated temperature [29]. Similar to η_m, η_m^E increased as x_1 increased to the maximum then dropped to zero, as illustrated in Fig. 6. It should be noted that the maximum η_m^E was found to be independent of the temperature and can be located at $x_1 \sim 0.3$. In comparison with the conventional aqueous amine solutions at 313.15 K, aqueous DEAB solution is the only liquid mixture that possesses positive η_m^E over an entire concentration range. Some liquid mixtures (which are aqueous solutions of MEA, AMP, and MDEA) show both positive and negative values of η_m^E. This refers that the contraction of the three mixtures is dominated by both intermolecular interaction and molecular packing. The intermolecular interaction will dominate in a region of positive η_m^E, while the suitable molecular compactness will be more important in a region of negative η_m^E. In the case of DEA (which shows all negative η_m^E), its contraction is majorly

affected by a preference of the molecular compactness in the liquid mixture.

$$\eta_m^E = \eta_m - \sum_{i=1}^{n}(x_i\eta_i^0) \tag{21}$$

$$\eta_m^E = (2x_1 - 1)\sum_{k=1}^{m}\left[C_k(2x_1 - 1)^{k-1}\right] \tag{22}$$

$$C_k = \sum_{k'=1}^{m'}\left[c_{k'}T^{k'-1}\right] \tag{23}$$

The predictive correlation based on the Redlich-Kister equation for η_m^E can be written in Eq. (22) as a function of x_1 and temperature dependent coefficient C_k ($m = 5$). Based on the presented η_m^E data in Table 6, C_k can be obtained from a non-linear regression analysis and correlated as a polynomial equation of Eq. (23) with ($m' = 4$). The regressed constant parameters $c_{k'}$ for each C_k are listed in Table 7. As a result, the predicted η_m^E are plotted as the color solid lines against the η_m^E data, which are obtained from Eq. (21), in Fig. 6. It was found that they both agreed well with each other with %AAD of 2.35% and $\sigma(\eta_m^E)$ of 0.56 mPa.s. Regarding the developed predictive correlation for η_m^E, the predicted η_m can be obtained from Eq. (21). The results showed that the predicted η_m (color dashed lines) well corresponded with the experimental η_m (triangles) as shown in Fig. 5 with %AAD of 1.34% and $\sigma(\eta_m)$ of 0.56 mPa.s.

In this work, the third order polynomial function ($m' = 4$) was used to correlate the temperature dependent coefficient C_k with the temperature T, as shown in Eq. (23). Typically, the second order polynomial function ($m' = 3$) is used to avoid the data overfitting. However, it was observed in this study that C_k changed with T and reached a plateau as the temperature increased. Since this temperature dependency is well represented by the third order polynomial correlation, $m' = 4$ was used in Eq. (23). In comparison with the third order polynomial correlation ($m' = 4$), the second order polynomial correlation ($m' = 3$) shows a poorer prediction performance in that as m' is reduced from 4 to 3, (i) % AADs for η_m^E and η_m increase from 1.34% to 4.19% and from 2.35% to 6.53%, respectively and (ii) $\sigma(\eta_m^E)$ and $\sigma(\eta_m)$ increase from 0.56 mPa.s to 1.26 mPa.s.

3.2.2. Activation energy for viscous flow

An activation energy for viscous flow (or a Gibbs free energy for activation of viscous flow, ΔG^*, regarding Eyring activation energy [33]) of the pure DEAB can be determined based on the Arrhenius equation. Fig. S1 (in the Supplementary Material) shows that ΔG^* of the pure DEAB is 18.99 kJ/mol (which is much lower than that of the conventional amines) and can be ranked as DEAB < MEA < MDEA < DEA < AMP. This observation agrees well with the viscosity of pure amine (given in Fig. 5 at $x_i = 1.0$) and the literature data [21, 27-29, 31].

In the case of binary DEAB and water mixture, the mixture's viscosity was applied in Eq. (24). Based on this equation, it can be seen that η_m is contributed from the two terms which are (i) free volume effect ($\frac{hN_A}{V_m}$) and (ii) free energy for activation of viscous flow ($exp\left(\frac{\Delta G^*}{RT}\right)$). To investigate the effects of temperature and amine content on these two terms, plots of (i) $\frac{hN_A}{V_m}$ and (ii) $exp\left(\frac{\Delta G^*}{RT}\right)$ versus x_1 at various temperatures (Figs. 7 and 8) were constructed. It was observed from Fig. 7 that $\frac{hN_A}{V_m}$ was rarely affected by the temperature but sharply dropped ($x_1 < 0.2$) and slowly decreased ($x_1 > 0.2$) as x_1 increased. Hence, it can be said that a change of the amine content is a major contribution of the free volume effect ($\frac{hN_A}{V_m}$). For Fig. 8, it was found that both temperature and amine content influenced the free energy term ($exp\left(\frac{\Delta G^*}{RT}\right)$). Interestingly, an amine content dependency on $exp\left(\frac{\Delta G^*}{RT}\right)$ considerably dropped as the temperature increased from 298.15 K to 343.15 K. In other words, a change of $exp\left(\frac{\Delta G^*}{RT}\right)$ with x_1 was significant at 298.15 K while rarely noticed at 343.15 K.

$$\eta_i^0 \text{ or } \eta_m = \frac{hN_A}{V_m}exp\left(\frac{\Delta G^*}{RT}\right) \tag{24}$$

where h is Planck's constant, N_A is Avogadro's number, and R is universal gas constant

Even though both $\frac{hN_A}{V_m}$ and $exp\left(\frac{\Delta G^*}{RT}\right)$ affect η_m, the latter term is a major contributor since it covers the influences of both temperature and amine concentration. To be further investigated, ΔG^* (which is a good representation of the viscous flow resistance) should be considered. By applying the same analogy of the thermodynamics Gibbs free energy, ΔG^* can be associated with the two temperature independent parameters, which are the enthalpy for activation of viscous flow (ΔH^*) and the entropy for activation of viscous flow (ΔS^*), as given in Eq. (25) [24]. Combining Eqs. (24) and (25), ΔH^* and ΔS^* can be determined from a plot of $\ln\left(\frac{\eta_m V_m}{hN_A}\right)$ and $1/T$ (see Eq. (26)). Based on the experimental η_m data (presented in Table 6), ΔH^* and ΔS^* were calculated and presented in Table S2 (in the Supplementary Material). As a result, ΔG^* can then be determined from Eq. (25).

$$\Delta G^* = \Delta H^* - T\Delta S^* \tag{25}$$

$$\ln\left(\frac{\eta_m V_m}{hN_A}\right) = \frac{\Delta H^*}{RT} - \frac{\Delta S^*}{R} \tag{26}$$

It was observed that ΔG^* of a binary DEAB and water mixture (shown in Table S2 and Fig. S2 in the Supplementary Material) very slightly decreased as the temperature increased but noticeably changed as the amine content was varied. In other words, the amine content played a key role on ΔG^*. This observation gives a better understanding on the free energy term $exp\left(\frac{\Delta G^*}{RT}\right)$ in that its amine content dependence is contributed from ΔG^*, while its temperature dependence majorly associates with the inverse temperature ($1/T$).

Bearing in mind that ΔH^* and ΔS^* are the temperature independent parameters, a slightly decrease of ΔG^* (as the temperature increases) is a result of $T\Delta S^*$ in Eq. (25). Since ΔH^* is greater than $T\Delta S^*$(as shown in Table S2 in the Supplementary Material), ΔG^* is then found to be positive. Thus, it can be implied that ΔH^* is the main parameter affecting ΔG^*. The literature also suggested that positive ΔG^* and ΔH^* indicated a strong intermolecular force and/or a preference molecular packing in

Table 7
Constant parameters for temperature dependent coefficient (C_k).

Temperature dependent coefficient (C_k)	Constant parameter	
C_1	c_1	1.99440×10^4
	c_2	-1.78514×10^2
	c_3	5.33395×10^{-1}
	c_4	-5.31872×10^{-4}
C_2	c_1	-4.98187×10^4
	c_2	4.48380×10^2
	c_3	-1.34601
	c_4	1.34747×10^{-3}
C_3	c_1	2.63869×10^4
	c_2	-2.37933×10^2
	c_3	7.15859×10^{-1}
	c_4	-7.18425×10^{-4}
C_4	c_1	5.00803×10^4
	c_2	-4.50855×10^2
	c_3	1.35226
	c_4	-1.35130×10^{-3}
C_5	c_1	-5.12449×10^4
	c_2	4.62307×10^2
	c_3	-1.38992
	c_4	1.39256×10^{-3}

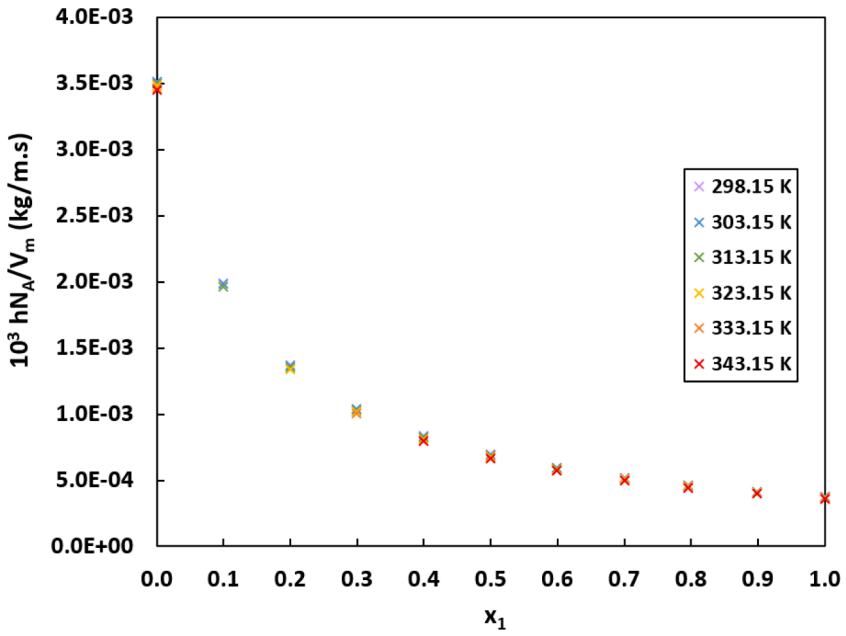

Fig. 7. Free volume effect (hN_A/V_m) of aqueous DEAB solution at various concentrations and temperatures.

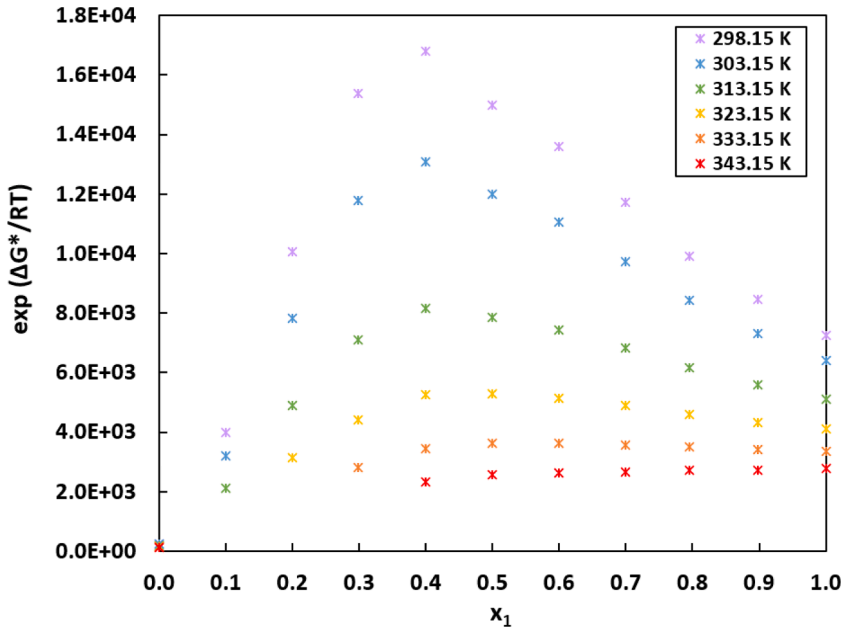

Fig. 8. Free energy for activation of viscous flow ($exp(\Delta G^*/RT)$) of aqueous DEAB solution at various concentrations and temperatures.

the liquid mixture [24, 28]. This observation is well corresponding with the liquid contraction of binary DEAB and water mixture, as discussed for V_m^E and η^E. Table S2 and Fig. S2 (in the Supplementary Material) also show that ΔH^* and ΔS^* clearly exhibit the maximum point (at $x_1 \sim 0.3$), which is close to the maximum liquid viscosity (see Fig. 5). Regarding a disorder-order plot (Fig. S3 in the Supplementary Material), an addition of water into the pure DEAB increases the liquid molecular randomness or the liquid disorder [34]. This increment is maximized at $x_1 \sim 0.3$ then decreases to the randomness level of the pure water. Interestingly, the maximum liquid disorder and the maximum liquid viscosity are found to be at the same amine content of $x_1 \sim 0.3$.

In this work, the Redlich-Kister based correlation was developed to estimate ΔG^* through an excess Gibbs free energy for activation of viscous flow (ΔG^{*E}), which is defined as a deviation of ΔG^* between real and ideal liquid mixtures, as shown in Eq. (27) [35]. Based on the presented volumetric and viscometric data of the liquid mixture and the pure liquid, ΔG^{*E} can be determined and presented in Table S3 (in the Supplementary Material) and Fig. 9.

$$\Delta G^{*E} = RT\ln\left(\frac{\eta_m V_m}{hN}\right) - \left(x_1 RT\ln\left(\frac{\eta_1^0 V_1^0}{hN}\right) + x_2 RT\ln\left(\frac{\eta_2^0 V_2^0}{hN}\right)\right) \quad (27)$$

The results showed that ΔG^{*E} data were positive over an entire range of amine content and a studied range of temperature. This can be implied that ΔG^* of the real liquid mixture is greater than that of the ideal liquid mixture. In other words, the real liquid has higher viscous flow resistance than the ideal liquid. It is due to a contraction of the liquid mixture. The given reason is in good agreement with the literature in that the positive value of ΔG^{*E} refers that there is a strong interaction

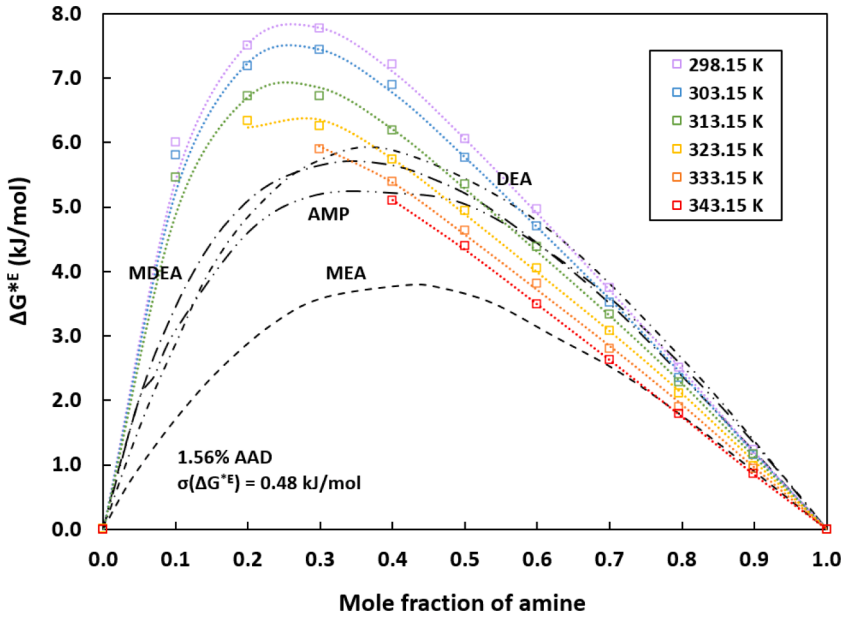

Fig. 9. ΔG^{*E} of aqueous solutions of DEAB over ranges of concentration and temperature; open squares are data obtained from Eq. (27), color dashed lines are predicted results from Redlich-Kister equation, and black dashed lines are ΔG^{*E} of conventional amines at 313.15 K [21, 36, 37].

between the unlike molecules (in this case, DEAB and water) [34]. One should be pointed out that the contraction of the liquid mixture is also confirmed by the negative values of V_m^E and positive values of η_m^E, ΔG^*, and ΔH^*, as shown in Figs. 2 and 6 and Fig. S2 (in the Supplementary Material), respectively. Since the influence of the amine content on ΔG^* was greater than that of the temperature, ΔG^{*E} was then found to be more dependent on the amine content rather than the temperature, as shown in Fig. 9. Additionally, the maximum ΔG^{*E} and the maximum η_m^E were observed at the same amine content, approximately 0.3. These given results confirm that ΔG^{*E} strongly associates with η_m^E.

The Redlich-Kister equation for ΔG^{*E} and its corresponding temperature dependent parameters D_k can be written as Eqs. (28) and (29), respectively. Based on the non-linear regression analysis, the constant parameters $d_{k'}$ can be determined ($m = 4$ and $m' = 3$), as given in Table 8. It was found that the predicted ΔG^{*E} (plotted as the color dashed lines in Fig. 9) was concordance well with the ΔG^{*E} obtained from Eq. (27) (presented as the open squares) with %AAD of 1.56% and $\sigma(\Delta G^{*E})$ of 0.49 kJ/mol. In comparison with the conventional binary amine and water mixtures (see Fig. 9), the aqueous solution of DEAB was found to have higher ΔG^{*E}. In other words, DEAB mixture possessed larger deviation from the ideal mixture than DEA, MDEA, AMP, and MEA, respectively. In accordance with the predicted ΔG^{*E}, the predicted ΔG^* can be determined from Eqs. (24) and (27), the predicted ΔG^* data are plotted as the color dashed lines in Fig. S2 (in the Supplementary Material). The predicted ΔG^* data are correspondingly well with ΔG^* obtained from Eq. (25) with %AAD of 0.43% and $\sigma(\Delta G^*)$ of 0.48 kJ/mol.

Table 8
Constant parameters for temperature dependent coefficient (D_k).

Temperature dependent coefficient (D_k)	Constant parameter	
D_1	d_1	2.4391×10^2
	d_2	-1.2459
	d_3	1.7067×10^{-3}
D_2	d_1	-3.2871×10^2
	d_2	1.8060
	d_3	-2.6124×10^{-3}
D_3	d_1	-2.6267×10^2
	d_2	1.8758
	d_3	-3.1162×10^{-3}
D_4	d_1	2.1362×10^2
	d_2	-1.4706
	d_3	2.4094×10^{-3}

$$\Delta G^{*E} = (2x_1 - 1)\sum_{k=1}^{m}\left[D_k(2x_1 - 1)^{k-1}\right] \tag{28}$$

$$D_k = \sum_{k'=1}^{m'}\left[d_{k'}T^{k'-1}\right] \tag{29}$$

$$\Delta S^{*E} = \left(\frac{\partial \Delta G^{*E}}{\partial T}\right)_{x_i,P} \tag{30}$$

In addition to ΔG^{*E}, the excess entropy for activation of viscous flow (ΔS^{*E}) can be determined through Eq. (30). The obtained ΔS^{*E} are plotted in Fig. S4 (in the Supplementary Material) against the literature data of the conventional amine solutions [21, 36]. Since ΔS^* is a temperature independent parameter, ΔS^{*E} (which is a deviation of ΔS^* between the real and ideal mixtures) was then found to be independent of the temperature but varied with the amine content. Even though ΔS^* was not a key parameter influencing ΔG^* but ΔH^* (as previously mentioned), ΔS^* contributed to (i) a slightly decrease of ΔG^* as the temperature increased and (ii) a molecular randomness for activation of viscous flow. Based on the definition of ΔS^{*E}, the positive values in the case of DEAB aqueous solution infers that the real DEAB mixture has higher level of molecular randomness for activation of viscous flow than the ideal DEAB mixture. Additionally, Fig. S4 (in the Supplementary Material) shows that ΔS^{*E} of DEAB is larger than that of MDEA, AMP, DEA, and MEA, respectively. Hence, the deviation of a real mixture from an ideal mixture for the molecular randomness for activation of viscous flow can be ordered as: DEAB > MDEA > AMP > DEA > MEA.

3.3. Refractive index

The collected experimental refractive index (n_D) for aqueous DEAB solution over studied ranges of temperature and concentration are tabulated in Table 9 and plotted as the color diamonds in Fig. 10. The results showed that n_D of a binary DEAB and water mixture sharply increased as the DEAB content increased within a range of x_1 less than 0.3 but very slightly increased and almost reached constant over x_1 of 0.3-1.0. It can be implied from this observation that the speed of light

Table 9
n_D and n_D^E of binary mixture of DEAB (1) and water (2) at various temperatures.

x_1	n_D [(a)] 298.15 K	n_D^E	n_D [(a)] 303.15 K	n_D^E	n_D [(a)] 313.15 K	n_D^E
0.0000	1.33251	0.0000	1.33194	0.0000	1.33063	0.0000
0.1000	1.39692	0.0543	1.39537	0.0534	1.39181	0.0515
0.1999	1.42002	0.0672	1.41801	0.0661	1.41388	0.0639
0.2989	1.42809	0.0653	1.42607	0.0643	1.42144	0.0618
0.4000	1.43226	0.0592	1.43003	0.0581	1.42553	0.0561
0.5000	1.43392	0.0507	1.43168	0.0498	1.42714	0.0480
0.5991	1.43481	0.0415	1.43258	0.0408	1.42803	0.0393
0.6999	1.43515	0.0316	1.43294	0.0311	1.42843	0.0300
0.7955	1.43492	0.0217	1.43273	0.0213	1.42829	0.0205
0.8983	1.43448	0.0109	1.43233	0.0106	1.42797	0.0103
1.0000	1.43394	0.0000	1.43187	0.0000	1.42757	0.0000

x_1	n_D [(a)] 333.15 K	n_D^E	n_D [(a)] 343.15 K	n_D^E
0.0000	1.32907	0.0000	1.32729	0.0000
0.1000	N/A	N/A	N/A	N/A
0.1999	N/A	N/A	N/A	N/A
0.2989	1.41717	0.0599	N/A	N/A
0.4000	1.42107	0.0543	1.41641	0.0524
0.5000	1.42259	0.0464	1.41793	0.0448
0.5991	1.42350	0.0380	1.41900	0.0368
0.6999	1.42395	0.0289	1.41937	0.0279
0.7955	1.42387	0.0198	1.41933	0.0191
0.8983	1.42364	0.0099	1.41921	0.0095
1.0000	1.42333	0.0000	1.41901	0.0000

N/A: not applicable due to phase separation of the solvent
Standard uncertainties: $u(x) = 0.0002$, $u(T) = 0.006\ K$, $u(w) = 0.00008\ g$, and $u(rep) = 0.00005$
Combined expanded uncertainties: $U_c(n_D) = 0.0001$ and $U_c(n_D^E) = 0.0002$ with 0.95 level of confidence (k ≈ 2)
[(a)] Data obtained from Maneeintr et al. [10].

significantly decreased as increasing x_1 from 0.0 to 0.3 but rarely changes within 0.3-1.0 range of x_1. Since the light travels slower as the liquid density increases, n_D then increases as increasing ρ_m [38]. The above-mentioned behavior of n_D well corresponds with a large decrease of ρ_m over a low range of x_1 and a slight reduction of ρ_m over a high range of x_1, as shown in Fig. 1. The relationship between n_D and ρ_m is also presented in Fig. S5 (in the Supplementary Material). Additionally, it can be observed that n_D slightly decreases as increasing the temperature, which is a typical behavior of the liquid amine solution [39–42]. It was also found that n_D of the aqueous DEAB solution was in the same range with that of the conventional aqueous amine solution at 303.15 K. Aqueous solution of DEAB had slightly lower n_D than that of MEA, AMP, MDEA, and DEA, respectively (see Fig. 10).

Since there is an association between n_D and ρ_m, the molar polarizability (R_m) is then defined to take both parameters into account. Based on the Lorenz-Lorenz equation, R_m can be written as Eq. (31) [43]. It should be noted that R_m not only represents the molar refraction of liquid mixture but is also considered as a spherical hard-core volume associated with the electronic polarization [44]. In this regard, the molar free volume (f_m), which is an unoccupied liquid molar volume, can be defined as Eq. (32) [45]. Based on the experimental density and refractive index data, R_m and f_m of the aqueous DEAB solution over an entire range of amine content and a temperature range of 298.15-343.15 K can be calculated and presented in Table S4 and Fig. S6 (in the Supplementary Material). It was found that f_m considerably decreased as ρ_m increased but slightly increased as the temperature increased. The obtained information is useful for a consideration of the physical solubility of CO_2 in the liquid mixture in that the solubility increases as f_m increases. This trend follows a typical behavior of the physical CO_2 solubility in the liquid mixture reported in the literature [46].

$$R_m = \left(\frac{n_D^2 - 1}{n_D^2 + 2}\right) V_m \tag{31}$$

$$f_m = V_m - R_m \tag{32}$$

Regarding the experimental n_D of the pure DEAB, the predictive correlation can be developed, as shown in Eq. (33). It was found that the predicted results were in a very good agreement with the experimental data with %AAD of 0.05% and $\sigma(n_D)$ of 0.0009. For the aqueous DEAB solution, the Redlich-Kister equation for excess refractive index (n_D^E) was applied. As shown in Eq. (34), n_D^E can be determined by subtracting the refractive index of a real mixture (n_D) with that of an ideal mixture ($\sum_{i=1}^{n}(x_i n_{Di}^0)$). As a result, n_D^E over ranges of the studied concentration and temperature were reported in Table 9 and Fig. 11. It was seen that n_D^E slightly decreased as the temperature increased. On the other hand, a more considerably variation of n_D^E was observed when the amine content was varied. To be more specific, n_D^E of the aqueous DEAB solution sharply increased to the maximum point at $x_1 \sim 0.25$ then rapidly

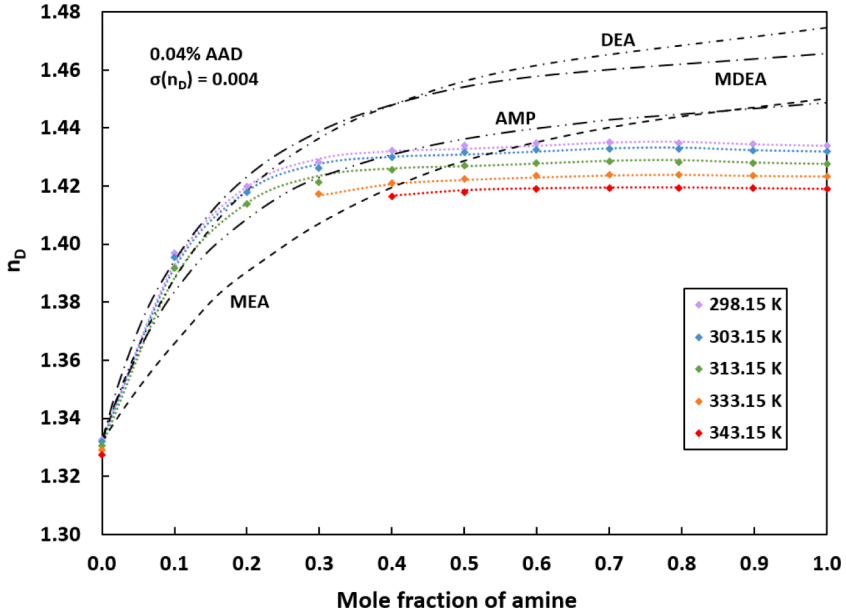

Fig. 10. n_D of aqueous solutions of DEAB over ranges of concentration and temperature; diamonds are experimental data, color dashed lines are predicted results, and black dashed lines are n_D of conventional amines at 303.15 K [41, 42, 47].

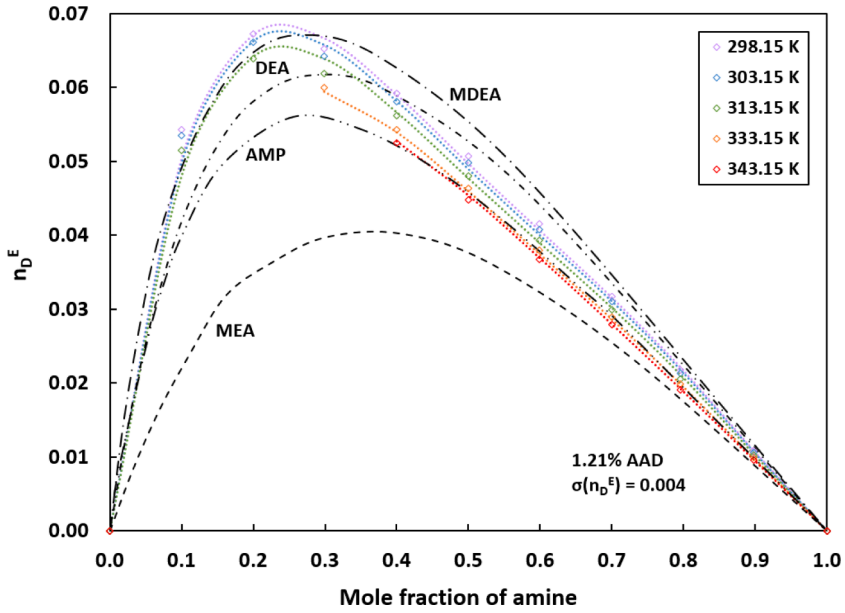

Fig. 11. n_D^E of aqueous solutions of DEAB over ranges of concentration and temperature; open diamonds obtained from Eq. (34), color dashed lines are predicted results from the Redlich-Kister equation, and black dashed lines are n_D of conventional amines at 303.15 K [41, 42, 47].

dropped to zero at $x_1 = 1.0$.

$$n_{D1}^0 = (1.5278) - \left(3.1435 \times 10^{-4}\right)T \tag{33}$$

$$n_D^E = n_D - \sum\nolimits_{i-1}^{n} x_i n_{Di}^0 \tag{34}$$

$$n_D^E = (2x_1 - 1)\sum_{k=1}^{m}\left[E_k(2x_1 - 1)^{k-1}\right] \tag{35}$$

$$E_k = \sum_{k'=1}^{m'}\left[e_{k'}T^{k'-1}\right] \tag{36}$$

Based on the Redlich-Kister equation, n_D^E can be correlated with x_1 and temperature dependent coefficient E_k, as given in Eq. (35). From the non-linear regression analysis, E_k can be written as a polynomial function with temperature and constant parameters $e_{k'}$, as shown in Eq. (36). As a results, $e_{k'}$ for each E_k can be tabulated in Table 10 with $m = 4$ and $m' = 3$. The predicted n_D^E from the Redlich-Kister equation are presented as the color dashed lines in Fig. 11. There is a concordance between the predicted n_D^E and that obtained from Eq. (34) with %AAD of 1.21% and $\sigma(n_D^E)$ of 0.004. Regarding Eq. (34), the predicted n_D can be determined. Fig. 10 shows that the predicted n_D very well fits with the experimental n_D with %AAD of 0.04% and $\sigma(n_D)$ of 0.004.

Table 10
Constant parameters for temperature dependent coefficient (E_k).

Temperature dependent coefficient (E_k)	Constant parameter	
E_1	e_1	8.4531×10^{-1}
	e_2	-3.7284×10^{-3}
	e_3	5.2298×10^{-6}
E_2	e_1	-1.3984×10^{-1}
	e_2	-7.3420×10^{-4}
	e_3	1.9425×10^{-6}
E_3	e_1	-3.4422
	e_2	2.4750×10^{-2}
	e_3	-4.1830×10^{-5}
E_4	e_1	3.6622
	e_2	-2.5525×10^{-2}
	e_3	4.2841×10^{-5}

3.4. Application in CO_2 capture

This work presented the fundamental physical properties of a binary DEAB and water mixture as well as their excess and associated properties. ρ_m, η_m, V_m, and α_m are essential for the experiment [48–50] and the simulation [51–53] of the hydrodynamics of an aqueous amine solution in the absorption column. Since DEAB has not yet been commercially available, its fluid properties (which can be obtained from the proposed correlations) need to be custom imported to the commercial simulation software. In addition to the fluid hydrodynamics, these fundamental properties are crucial for the CO_2 absorption kinetics and mass transfer modelling [12, 52]. Since the refractive index of an aqueous DEAB solution changes with the amine content and temperature, the measurement of liquid refractive index can be alternatively used to determine the amine concentration in substitution of the typical acidification method [54]. Additionally, f_m (which can be derived from density and refractive index) is a good indicating parameter for the physical solubility of CO_2 in the aqueous amine solution [55].

Even though the presented excess properties reveal the strong molecular interaction and the suitable molecular packing in the liquid mixture, the computational molecular simulation (e.g., density function theory or DFT [56] and *Ab Initio* molecular dynamics [57]) and the spectral characteristics molecular interaction study (e.g., infrared spectroscopy [58], fluorescence spectroscopy [59], and nuclear magnetic resonance spectroscopy [60]) should be applied for a better understanding of the interaction between DEAB and water.

Although DEAB was previously proposed by Maneeintr and co-workers [10] as a high potential amine for the CO_2 capture application, its physical properties (i.e., density, viscosity, and refractive index) was just reported and estimated over an entire range of DEAB content and a temperature range of 298.15-343.15 K. Several associated properties have not yet been reported and discussed for a better understanding of binary DEAB and water mixture. Their Redlich-Kister correlations for V_m^E, η_m^E, and n_D^E were also applicable at specific temperatures of 298.15, 303.15, 313.15, 323.15, 333.15, and 343.15 K. This can be implied that Maneeintr and co-workers [10] aimed at reporting the experimental measured densities, viscosities, and refractive indices and correlating their excess properties using the Redlich-Kister equation.

In this work, the additional volumetric, viscometric, and refraction

properties (including $\overline{V}_i$, $\overline{V}_i^{\infty}$, $V_{\varphi,i}$, $V_{\varphi,i}^{\infty}$, α_m, α_m^E, ΔG^*, ΔG^{*E}, ΔH^*, ΔS^*, ΔS^{*E}, R_m, and f_m) were reported and comprehensively discussed for new insights of the liquid mixture. In comparison with the correlations (which were proposed by Maneeintr and colleagues [10]), the updated correlations (reported in this study) can well be used to estimate the density, viscosity, and refractive index of a binary DEAB and water mixture over a whole range of amine concentration and a temperature range of 298.15-343.15 K without an interpolation to the desired temperature. However, a slight increase of %AADs was observed for the predictions of density (from 0.03% to 0.05 %), viscosity (from 0.88% to 1.34%), and refractive index (from 0.01% to 0.04%).

4. Conclusion

Fundamental physical properties of the aqueous DEAB solution over an entire range of amine content and a temperature range of 298.15-343.15 K were discussed. Based on the experimental ρ_m, η_m, and n_D, several associated physical properties can be further determined. They were (i) the volumetric properties of V_m, V_m^E, $\overline{V}_i$, $\overline{V}_i^{\infty}$, $V_{\varphi,i}$, $V_{\varphi,i}^{\infty}$, α_m, and α_m^E, (ii) the viscometric properties of η_m^E, ΔG^*, ΔH^*, ΔS^*, ΔG^{*E}, ΔS^{*E}, and (iii) the refraction properties of n_D^E, R_m, and f_m. This information was found to be very useful for a better understanding of the liquid mixture behavior. Contraction of the real liquid (by the intermolecular interaction and/or the suitable molecular compactness) was confirmed by the deviations of V_m^E, η_m^E, ΔG^{*E}, and n_D^E from the ideal mixture as well as the positive values of ΔG^* and ΔH^*. Typically, ρ_m was measured in accordance with the kinematic viscosity for a calculation of η_m. It was observed in this work that n_D strongly associated with ρ_m. Hence, n_D was suggested to be measured along with ρ_m and η_m. As a result, R_m (which is a good representation of the molar refraction) and f_m (which is helpful for the physical CO_2 solubility) were obtained. In addition to an insight discussion on the physical properties, the Redlich-Kister based predictive correlations were presented for V_m^E, α_m^E, η_m^E, ΔG^{*E}, and n_D^E at %AAD of 2.75%, 2.26%, 2.35%, 1.56%, and 1.21%, respectively. Since there was a phase separation of the DEAB and water mixture at a low range of x_1 and a relatively high temperature range of 323.15-343.15 K, further investigation on the phase separation condition and mechanism should be considered.

CRediT authorship contribution statement

Teerawat Sema: Conceptualization, Methodology, Writing – original draft, Writing – review & editing, Project administration, Funding acquisition. **Hongxia Gao:** Writing – review & editing. **Zhiwu Liang:** Writing – review & editing. **Paitoon Tontiwachwuthikul:** Writing – review & editing. **Raphael O. Idem:** Writing – review & editing.

Declaration of Competing Interest

The authors declare that they have no known competing financial interests or personal relationships that could have appeared to influence the work reported in this paper.

Data Availability

Data will be made available on request.

Acknowledgements

Supports from Thailand Science Research and Innovation Fund Chulalongkorn University (CU_FRB65_bcg (17)_085_23_15) was acknowledged. This research was financially supported by Sci-Super VIII fund from Faculty of Science, Chulalongkorn University.

Supplementary materials

Supplementary material associated with this article can be found, in the online version, at doi:10.1016/j.fluid.2022.113565.

References

[1] M. Aengenheyster, Q.Y. Feng, F. van der Ploeg, H.A. Dijkstra, The point of no return for climate action: effects of climate uncertainty and risk tolerance, Earth Syst. Dyn. 9 (2018) 1085–1095, https://doi.org/10.5194/esd-9-1085-2018.
[2] J.M. Chen, Carbon neutrality: toward a sustainable future, Innovation 2 (3) (2021), 100127, https://doi.org/10.1016/j.xinn.2021.100127.
[3] L. Chen, G. Msigwa, M. Yang, A.I. Osman, S. Fawzy, D.W. Rooney, P.S. Yap, Strategies to achieve a carbon neutral society: a review, Environ. Chem. Lett. (2022), https://doi.org/10.1007/s10311-022-01435-8.
[4] P. Moser, G. Wiechers, S. Schmidt, J.G.M.S. Monteiro, E. Goetheer, C. Charalambous, A. Saleh, M. van der Spek, S. Garcia, ALIGN-CCUS: results of the 18-month test with aqueous AMP/PZ solvent at the pilot plant at Niederaussem – solvent management, emissions and dynamic behavior, Int. J. Greenhouse Gas Control 109 (2021), 103381, https://doi.org/10.1016/j.ijggc.2021.103381.
[5] C. Bruce, S. Giannaris, B. Jacobs, S. Janowczyk, W. Srisang, Post combustion CO_2 capture retrofit of Saskpower's Shand Power Station: capital and operating cost reduction of a 2nd generation capture facility, in: Proceeding of the 14th Greenhouse Gas Control Technologies Conference, 2018, https://doi.org/10.2139/ssrn.3366401.
[6] S. Giannaris, D. Janowczyk, J. Ruffini, K. Hill, B. Jacobs, C. Bruce, Y. Feng, W. Srisang, SaskPower's Boundary Dam Unit 3 carbon capture facility - the journey to achieving reliability, in: Proceeding of the 15th Greenhouse Gas Control Technologies Conference, 2021, https://doi.org/10.2139/ssrn.3820191.
[7] Z.H. Liang, W. Rongwong, H. Liu, K. Fu, H. Gao, F. Cao, R. Zhang, T. Sema, A. Henni, K. Sumon, D. Nath, D. Gelowitz, W. Srisang, C. Saiwan, A. Benamor, M. Al-Marri, H. Shi, T. Supap, C. Chan, Q. Zhou, M. Abu-Zahra, M. Wilson, W. Olsen, R. Idem, P. Tontiwachwuthikul, Recent progress and new developments in post-combustion carbon-capture technology with amine based solvents, Int. J. Greenhouse Gas Control 40 (2015) 26–54, https://doi.org/10.1016/j.ijggc.2015.06.
[8] T. Sema, A. Naami, R. Idem, P. Tontiwachwuthikul, Correlations for equilibrium solubility of carbon dioxide in aqueous 4-(diethylamino)-2-butanol solutions, Ind. Eng. Chem. Res. 50 (2011) 14008–14015, https://doi.org/10.1021/ie2008345.
[9] P. Tontiwachwuthikul, A.G.H. Wee, R. Idem, K. Maneeintr, G.J. Fan, A. Henni, A. Aroonwilas, A. Chakma, 2011. Method of capturing carbon dioxide from gas streams. United States Patent US7910078B2.
[10] K. Maneeintr, A. Henni, R.O. Idem, P. Tontiwachwuthikul, A.G.H. Wee, Physical and transport properties of aqueous amino alcohol solutions for CO_2 capture from flue gas streams, Process Saf. Environ. Prot. 86 (2008) 291–295, https://doi.org/10.1016/j.psep.2008.03.006.
[11] A. Naami, M. Edali, T. Sema, R. Idem, P. Tontiwachwuthikul, Mass transfer performance of CO_2 absorption into aqueous solutions of 4-diethylamino-2-butanol, monoethanolamine, and *N*-methyldiethanolamine, Ind. Eng. Chem. Res. 51 (2012) 6471–6479, https://doi.org/10.1021/ie2008357.
[12] T. Sema, A. Naami, Z. Liang, R. Idem, H. Ibrahim, P. Tontiwachwuthikul, 1D absorption kinetics modeling of CO_2–DEAB–H_2O system, Int. J. Greenhouse Gas Control 12 (2013) 390–398, https://doi.org/10.1016/j.ijggc.2012.11.023.
[13] S.L. Ellison, A. Williams, Quantifying Uncertainty in Analytical Measurement, third ed., Eurachem, 2012. UK.
[14] S. K. K. Narayanaswamy, A.V. Rayer, A. Henni, Volumetric properties, viscosities, refractive indices and surface tensions for (dimethylpropanolamine (DMPA) + water) mixtures from 298.15 K to 343.15 K Thermochim. Acta 543 (2012) 218–225, https://doi.org/10.1016/j.tca.2012.05.025.
[15] M. Pirdashti, K. Movagharnejad, P. Akbarpour, E.N. Dragoi, I. Khoiroh, Thermophysical properties and experimental and modeling density of alkanol + alkane mixtures using neural networks developed with differential evolution algorithm, Int. J. Thermophys. 41 (2020) 35, https://doi.org/10.1007/s10765-020-2609-y.
[16] J. Li, M. Mundhwa, A. Henni, Volumetric properties, viscosities, refractive indices, and surface tensions for aqueous Genosorb 1753 solutions, J. Chem. Eng. Data 52 (2007) 955–958, https://doi.org/10.1021/je600547b.
[17] E. Vataščin, M. Havlová, V. Dohnal, Phase equilibria and volumetric and viscosity behavior of the aqueous double salt ionic liquid [EMIM][SCN]$_x$[MeSO$_3$]$_{(1-x)}$, Fluid Phase Equilib. 548 (2021), 113199, https://doi.org/10.1016/j.fluid.2021.113199.
[18] J. Han, J. Jin, D.A. Eimer, M.C. Melaaen, Density of water (1) + monoethanolamine (2) + CO_2 (3) from (298.15 to 413.15) K and surface tension of water (1) + monoethanolamine (2) from (303.15 to 333.15) K, J. Chem. Eng. Data 57 (2012) 1095–1103, https://doi.org/10.1021/je2010038.
[19] Y. Maham, T.T. Teng, A.E. Mather, L.G. Hepler, Volumetric properties of (water + diethanolamine) systems, Can. J. Chem. 73 (1995) 1514–1519, https://doi.org/10.1139/v95-187.
[20] Y. Maham, T.T. Teng, L.G. Hepler, A.E. Mather, Densities, excess molar volumes, and partial molar volumes for binary mixtures of water with monoethanolamine, diethanolamine, and triethanolamine from 25 to 80°C, J. Solution Chem. 23 (1994) 195–205, https://doi.org/10.1007/BF00973546.
[21] A. Henni, J.J. Hromek, P. Tontiwachwuthikul, A. Chakma, Volumetric properties and viscosities for aqueous AMP solutions from 25°C to 70°C, J. Chem. Eng. Data 48 (2003) 551–556, https://doi.org/10.1021/je0201119.

[22] A. Rezaei, P. Pakzad, M. Mofarahi, A.A. Izadpanah, M. Afkhamipour, C.H. Lee, Densities and viscosities of binary and ternary solutions of triethylenetetramine, 2-amino-2-methyl-1-propanol, and water for carbon dioxide capture, J. Chem. Eng. Data 66 (2021) 2942–2958, https://doi.org/10.1021/acs.jced.0c01052.
[23] M. Stec, A. Tatarczuk, D. Śpiewak, A. Wilk, Densities, excess molar volumes, and thermal expansion coefficients of aqueous aminoethylethanolamine solutions at temperatures from 283.15 to 343.15 K, J. Solution Chem. 43 (2014) 959–971, https://doi.org/10.1007/s10953-014-0175-2.
[24] S.S. Karunarathne, D.A. Eimer, L.E. Øi, Density, viscosity, and excess properties of MDEA + H_2O, DMEA + H_2O, and DEEA + H_2O mixtures, Appl. Sci. 10 (2020) 3196, https://doi.org/10.3390/app10093196.
[25] Y. Zhang, J. Yang, B. Li, K. Liu, X. Xie, J. Zhang, Density, viscosity, surface tension of 1,3-propanediol + dimethyl sulfoxide mixed solutions and their intermolecular forces from spectra and computational chemistry, Fluid Phase Equilib. 534 (2021), 112965, https://doi.org/10.1016/j.fluid.2021.112965.
[26] A. Muhammad, M.I.A. Mutalib, T. Murugesan, A. Shafeeq, Density and excess properties of aqueous *N*-methyldiethanolamine solutions from (298.15 to 338.15) K, J. Chem. Eng. Data 53 (2008) 2217–2221, https://doi.org/10.1021/je800416y.
[27] T.G. Amundsen, L.E. Øi, D.A. Eimer, Density and viscosity of monoethanolamine + water + carbon dioxide from (25 to 80)°C, J. Chem. Eng. Data 54 (2009) 3096–3100, https://doi.org/10.1021/je900188m.
[28] U.S.P.R. Arachchige, N. Aryal, D.A. Eimer, M.C. Melaaen, Viscosities of pure and aqueous solutions of monoethanolamine (MEA), diethanolamine (DEA) and *N*-methyldiethanolamine (MDEA), Annu. Trans. Nord. Rheol. Soc. 21 (2013) 299–306.
[29] J.M. Bernal-García, L.A. Galicia-Luna, K.R. Hall, M. Ramos-Estrada, G.A. Iglesias-Silva, Viscosities for aqueous solutions of N-methyldiethanolamine from 313.15 to 363.15 K, J. Chem. Eng. Data 49 (2004) 864–866, https://doi.org/10.1021/je0302250.
[30] N. Azarang, K. Movagharnejad, M. Pirdashti, M. Ketabi, Densities, viscosities, and refractive indices of poly(ethylene glycol) 300 + 1,2-ethanediol, 1,2-propanediol, 1,3-propanediol, 1,3-butanediol, or 1,4-butanediol binary liquid mixtures, J. Chem. Eng. Data 656 (2020) 3448–3462, https://doi.org/10.1021/acs.jced.9b01189.
[31] T.T. Teng, Y. Maham, L.G. Hepler, A.E. Mather, Viscosity of aqueous solutions of N-methyldiethanolamine and of diethanolamine, J. Chem. Eng. Data 39 (1994) 290–293, https://doi.org/10.1021/je00014a021.
[32] M.J. Lee, T.K. Lin, Density and viscosity for monoethanolamine+ water,+ ethanol, and+ 2-propanol, J. Chem. Eng. Data 40 (1995) 336–339, https://doi.org/10.1021/je00017a074.
[33] H. Eyring, Viscosity, plasticity, and diffusion as examples of absolute reaction rates, J. Chem. Phys. 4 (1936) 283–291, https://doi.org/10.1063/1.1749836.
[34] N. Ouerfelli, Z. Barhoumi, R. Besbes, N. Amdouni, The reduced Redlich–Kister excess molar Gibbs energy of activation of viscous flow and derived properties in 1,4-dioxane + water binary mixtures from 293.15 to 309.15 K, Phys. Chem. Liq. 49 (2011) 777–800, https://doi.org/10.1080/00319104.2010.521927.
[35] Z. Mousavi, M. Pirdashti, A.A. Rostami, E.N. Dragoi, Thermophysical properties analysis of poly (ethylene glycol) 600 + methanol, ethanol, 1-propanol, and 2-propanol binary liquid mixtures, Int. J. Thermophys. 41 (2020) 19, https://doi.org/10.1007/s10765-019-2600-7.
[36] Y. Maham, C.N. Liew, A.E. Mather, Viscosities and excess properties of aqueous solutions of ethanolamines from 25 to 80°C, J. Solution Chem. 31 (2002) 743–756, https://doi.org/10.1023/A:1021133008053.
[37] Y. Maham, L. Lebrette, A.E. Mather, Viscosities and excess properties of aqueous solutions of mono-and diethylethanolamines at temperatures between 298.15 and 353.15 K, J. Chem. Eng. Data 47 (2002) 550–553, https://doi.org/10.1021/je015528d.
[38] E. Silla, A. Arnau, I. TuñóN, Fundamental principles governing solvents use, in: G. Wypych (Ed.), Handbook of Solvents, ChemTec Publishing, Oxford, 2014, pp. 11–72.
[39] A.V. Rayer, S. Kadiwala, K. Narayanaswamy, A. Henni, Volumetric properties, viscosities, and refractive indices for aqueous 1-amino-2-propanol (monoisopropanolamine (MIPA)) solutions from (298.15 to 343.15) K, J. Chem. Eng. Data 55 (2010) 5562–5568, https://doi.org/10.1021/je100300s.
[40] D. Gómez-Díaz, M.D. La Rubia, A.B. López, J.M. Navaza, R. Pacheco, S. Sánchez, Density, speed of sound, refractive index, and viscosity of 1-amino-2-propanol {or bis (2-hydroxypropyl) amine}+ triethanolamine+ water from T=(288.15 to 333.15) K, Chem. Eng. Data 57 (2012) 1104–1111, https://doi.org/10.1021/je201121t.
[41] F.J. Tamajón, F. Cerdeira, E. Álvarez, Density, viscosity, and refractive index of N-methyldiethanolamine in blends of methanol + water as solvent and their binary systems from T = (293.15 to 323.15) K, J. Chem. Eng. Data 65 (2020) 4417–4434, https://doi.org/10.1021/acs.jced.0c00272.
[42] Y.M. Tseng, A.R. Thompson, densities and refractive indices of aqueous monoethanolamine, diethanolamine, triethanolamine, J. Chem. Eng. Data 9 (1964) 264–267, https://doi.org/10.1021/je60021a043.
[43] Ł. Marcinkowski, E. Szepiński, M.J. Milewska, A. Kloskowski, Density, sound velocity, viscosity, and refractive index of new morpholinium ionic liquids with amino acid-based anions: Effect of temperature, alkyl chain length, and anion, J. Mol. Liq. 284 (2019) 557–568, https://doi.org/10.1016/j.molliq.2019.04.026.
[44] M. Tariq, P.A.S. Forte, M.F.C. Gomes, J.N.C. Lopes, L.P.N. Rebelo, Densities and refractive indices of imidazolium- and phosphonium-based ionic liquids: Effect of temperature, alkyl chain length, and anion, J. Chem. Thermodyn. 41 (2009) 790–798, https://doi.org/10.1016/j.jct.2009.01.012.
[45] F. Hevia, A. Cobos, J.A. González. I.S. de la Fuente, L.S. Sanz, Thermodynamics of amide+ amine mixtures. 1. Volumetric, speed of sound, and refractive index data for N, N-dimethylformamide+ N-propylpropan-1-amine,+ N-butylbutan-1-amine, + butan-1-amine, or+ hexan-1-amine systems at several temperatures, J. Chem. Eng. Data 61 (2016) 1468–1478, https://doi.org/10.1021/acs.jced.5b00802.
[46] T. Sema, M. Edali, A. Naami, R. Idem, P. Tontiwachwuthikul, Solubility and diffusivity of N_2O in aqueous 4-(diethylamino)-2-butanol solutions for use in postcombustion CO_2 capture, Ind. Eng. Chem. Res. 51 (2012) 925–930, https://doi.org/10.1021/ie200832c.
[47] M. Ghulam, S.A. Mohd, B.M. Azmi, A. Faizan, Volumetric properties, viscosities and refractive indices of aqueous solutions of 2-amino-2-methyl-1-propanol (AMP), Res. J. Chem. Environ. 17 (2013) 22–31.
[48] S. Kouzbour, B. Gourich, Y. Stiriba, C. Vial, F. Gros, R. Sotudeh-Gharebagh, Experimental analysis of the effects of liquid phase surface tension on the hydrodynamics and mass transfer in a square bubble column, Int. J. Heat Mass Transfer 170 (2021), 121009, https://doi.org/10.1016/j.ijheatmasstransfer.2021.121009.
[49] A.B. López, M.D. La Rubia, J.M. Navaza, R. Pacheco, D. Gómez-Díaz, Carbon dioxide absorption in triethanolamine aqueous solutions: hydrodynamics and mass transfer, Chem. Eng. Technol. 37 (2014) 419–426, https://doi.org/10.1002/ceat.201300603.
[50] I. Iliuta, F. Larachi, CO_2 and H_2S absorption by MEA solution in packed-bed columns under inclined and heaving motion conditions - hydrodynamics and reactions performance for marine applications, Int. J. Greenhouse Gas Control 79 (2018) 1–13, https://doi.org/10.1016/j.ijggc.2018.09.016.
[51] J. Kim, D.A. Pham, Y.I. Lim, Gas−liquid multiphase computational fluid dynamics (CFD) of amine absorption column with structured-packing for CO_2 capture, Comput. Chem. Eng. 88 (2016) 39–49, https://doi.org/10.1016/j.compchemeng.2016.02.006.
[52] D. Sebastia-Saez, S. Gu, P. Ranganathan, K. Papadikis, 3D modeling of hydrodynamics and physical mass transfer characteristics of liquid film flows in structured packing elements, J. Greenhouse Gas Control 19 (2013) 492–502, https://doi.org/10.1016/j.ijggc.2013.10.013.
[53] M.F. Ali, J. Gan, X. Chen, G. Yu, Y. Zhang, M. Ellahi, A.A. Abdeltawab, Chem. Eng. Res. Des. 129 (2018) 356–375, https://doi.org/10.1016/j.cherd.2017.11.034.
[54] F. Pouryousefi, R.O. Idem, New analytical technique for carbon dioxide absorption solvents, nd. Eng. Chem. Res. 47 (2008) 1268–1276, https://doi.org/10.1021/ie0709786.
[55] S. Bishnoi, G.T. Rochelle, Physical and chemical solubility of carbon dioxide in aqueous methyldiethanolamine, Fluid Phase Equilib. 168 (2000) 241–258, https://doi.org/10.1016/S0378-3812(00)00303-4.
[56] J.X. Mao, H.B. Nulwala, D.R. Luebke, K. Damodaran, Spectroscopic and computational analysis of the molecular interactions in the ionic liquid ion pair $[BMP]^+[TFSI]^-$, J. Mol. Liq. 175 (2012) 141–147, https://doi.org/10.1016/j.molliq.2012.09.001.
[57] R. Ghanghas, A. Jindal, S. Vasudevan, Distinguishing intra- and intermolecular interactions in liquid 1,2-ethanediol by ^1H NMR and Ab Initio molecular dynamics, J. Phys. Chem. B 122 (2018) 9757–9762, https://doi.org/10.1021/acs.jpcb.8b07750.
[58] G.P. Dubey, P. Kaur, Thermodynamic and spectral studies of molecular interactions in binary liquid mixtures of 1-butoxy-2-propanol with 1-alcohols, Chem. Eng. Data 60 (2015) 2232–2239, https://doi.org/10.1021/acs.jced.5b00031.
[59] M. Homocianu, A. Airinei, Intra-/inter-molecular interactions – identification and evaluation by optical spectral data in solution, J. Mol. Liq. 225 (2017) 869–876, https://doi.org/10.1016/j.molliq.2016.11.013.
[60] S. Pradhan, S. Mishra, An eye on molecular interaction studies of non-aqueous binary liquid mixtures with reference to dielectric, refractive properties and spectral characteristics, J. Mol. Liq. 279 (2019) 317–326, https://doi.org/10.1016/j.molliq.2019.01.138.